EXPERIMENTAL STUDY OF MULTIPHASE PUMP WEAR

A Thesis

by

DANIEL D'ANDREA STECK

Submitted to the Office of Graduate and Professional Studies of
Texas A&M University
in partial fulfillment of the requirements for the degree of

MASTER OF SCIENCE

Chair of Committee,	Gerald L. Morrison
Committee Members,	Devesh Ranjan
	Robert E. Randall
Head of Department,	Andreas A. Polycarpou

August 2014

Major Subject: Mechanical Engineering

ABSTRACT

The goal of this research is to better understand upstream Oil & Gas Electric Submersible Pump (ESP) reliability issues. The objective of this research is to determine how Liquid-Gas-Particulate (LGP) turbine pump wear differs from Liquid-Particulate (LP) turbine pump wear. This objective is novel because little is known about LGP wear, yet such wear is common in ESPs. To accomplish the research objective, an experimental study of a gas handling ESP was conducted. Tests of two Baker Hughes 1025 MVP G400 Severe Duty turbine pumps were conducted with water, air, and sand. One pump was tested with a Gas Volume Fraction (GVF) of 20% while the other was tested with a GVF of 0%. It was found that particulates migrate radially outward through the pump and cause diffuser sidewall wear to increase through the pump. It was also found that various impeller flow path areas experience more LGP wear than LP wear. In general, pump wear progress faster for LGP wear than for LP wear. It is believed that this is caused primarily by the thinning effect that gas can have on a fluid's viscosity.

TABLE OF CONTENTS

LIST OF FIGURES

LIST OF TABLES

1. INTRODUCTION

This section provides motivation and background for the present study. The subsections are as follows:

- Electric Submersible Pump Reliability Issues
- Liquid-Gas-Particulate Turbine Pump Wear Existence
- Turbine Pump Components
- Liquid Pump Mechanics
- Liquid-Particulate Pump Wear Mechanisms
- Liquid-Particulate Pump Design
- Liquid-Particulate Turbine Pump Wear
- Liquid-Gas Pump Mechanics
- Liquid-Gas-Particulate Pump Wear

Electric Submersible Pump Reliability Issues

Electric Submersible Pumps (ESPs) presently produce 60% of the world's oil [1]. ESPs are selected for their high volume flow rates [2]. However, ESPs have serious reliability issues. While standard centrifugal pumps have fifteen to twenty-year run lives [3], ESPs often have two-year run lives [4]. Two-year ESP run lives are tolerable for onshore oil production because the onshore replacement cost is acceptable; however, two-year run lives are unacceptable for deepwater offshore oil production due to the high cost of replacement (with the largest costs being associated with production downtime and offshore workover rig rental) [4]. A goal of many operators is to increase average ESP run life to five years in the near term [1]. One study, summarized in Figure 1, found that turbine pump failures were responsible for 17% of ESP failures and that 17% of turbine pump failures were caused by particulates. This study aims to better understand how turbine pumps are damaged by particulates by investigating how the presence of gas affects turbine pump wear.

1
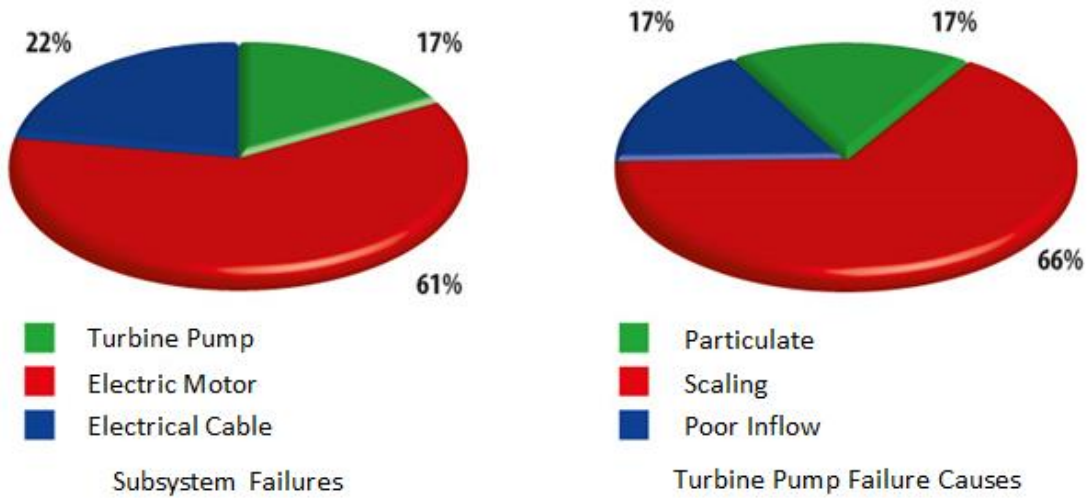
Figure 1. Distribution of ESP subsystem failures (left) and distribution of turbine pump failure causes (right) [5]

Liquid-Gas-Particulate Turbine Pump Wear Existence

ESPs are commonly used in the oil and gas industry to pump crude oil from underground formations [2]. An oil well equipped with an ESP is depicted in Figure 2. An electrical cable extends from the motor controller to the electric motor. Oil enters the well below the electric motor, flows over the motor and protector and into the turbine pump's intake. The turbine pump pressurizes the fluid enough to push it to the surface which can be up to 10,000 ft above [6]. Often times, natural gas will come up with the crude oil [2]. The percentage of gas volume flow rate to total volume flow rate, at the pump inlet, is referred to as Gas Volume Fraction (GVF) [7]. It is possible that in addition to crude oil and natural gas, a small concentration of solid particles could reach the turbine pump [2]. This situation leads to liquid-gas-particulate wear within the turbine pump.
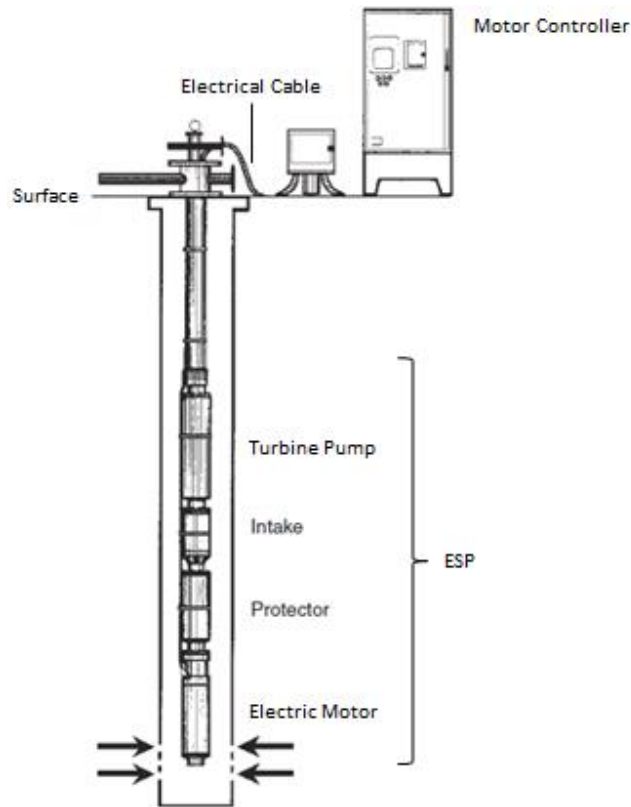
Figure 2. Oil well schematic (not drawn to scale) [2]

There are various types of solid particles that can come in contact with the turbine pump; however, the hardest and therefore most damaging type is silica sand (SiO$_2$) [2]. Common levels of silica sand observed in oil well streams are classified in Table 1.

Table 1. Common levels of silica sand observed in oil wells [2]

Level	Particle Concentration (% by weight)
Light	< 0.001
Moderate	$0.001 - 0.005$
Heavy	$0.005 - 0.020$
Severe	> 0.020

Turbine Pump Components

Figure 3 depicts some of the key components within a turbine pump. The depicted turbine pump has three stages, with each stage consisting of an impeller and a diffuser. Each impeller is rotated by the shaft and imparts energy to the fluid. The diffusers consist of stationary channels that direct the fluid to the next impeller and decrease the fluid velocity. The radial bearings support the rotating shaft.
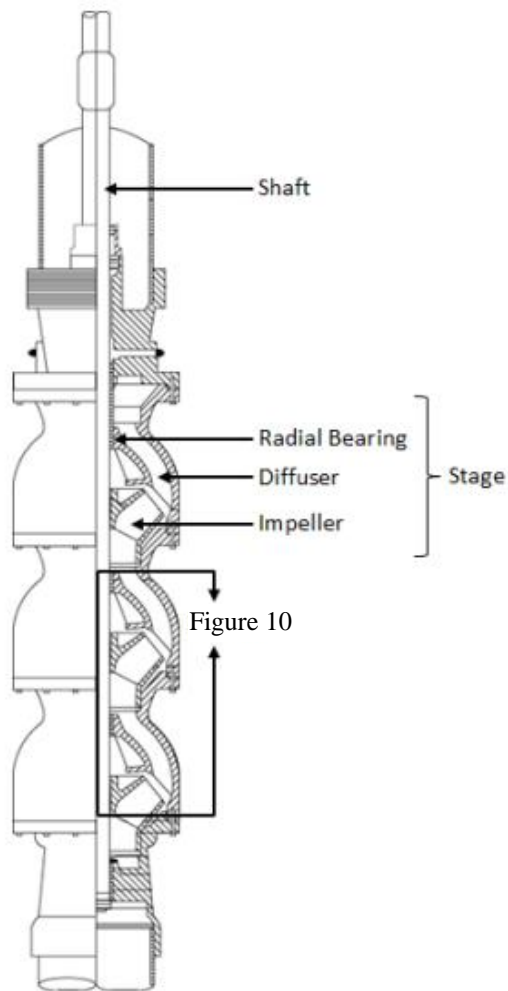
Figure 3. Three stage turbine pump [8]

Figure 4 depicts one mixed flow impeller and two adjoining diffusers from the turbine pump depicted in Figure 3. The impeller and diffuser flow paths are identified by the thick blue lines. The arrows point from inlet to outlet. The internal leakage flow paths are identified by the thin blue lines. The arrows show the direction of fluid leakage. Fluid leaks through clearances from the high pressure impeller outlet to the low pressure impeller inlet because of the pressure differential. Ring seals at the front and back of the impeller are used to minimize the leakage. The ring seal surfaces on the impeller mate with ring seal surfaces on the adjoining diffusers. The narrow ring seal gaps restrict the leakage flow. The ring seals also act as radial bearings. Under most conditions, the impeller experiences downward thrust because the outlet pressure is significantly higher than the inlet pressure. This downward thrust is minimized by allowing inlet pressure fluid into a cavity above the impeller through balance holes. The remaining downward thrust is transferred to the lower diffuser through the eye thrust bearing. At high flow rates and during pump startup, the change in momentum flux can dominate the pressure forces and produce an upward thrust. This thrust is transferred to the upper diffuser by the up-thrust bearing.
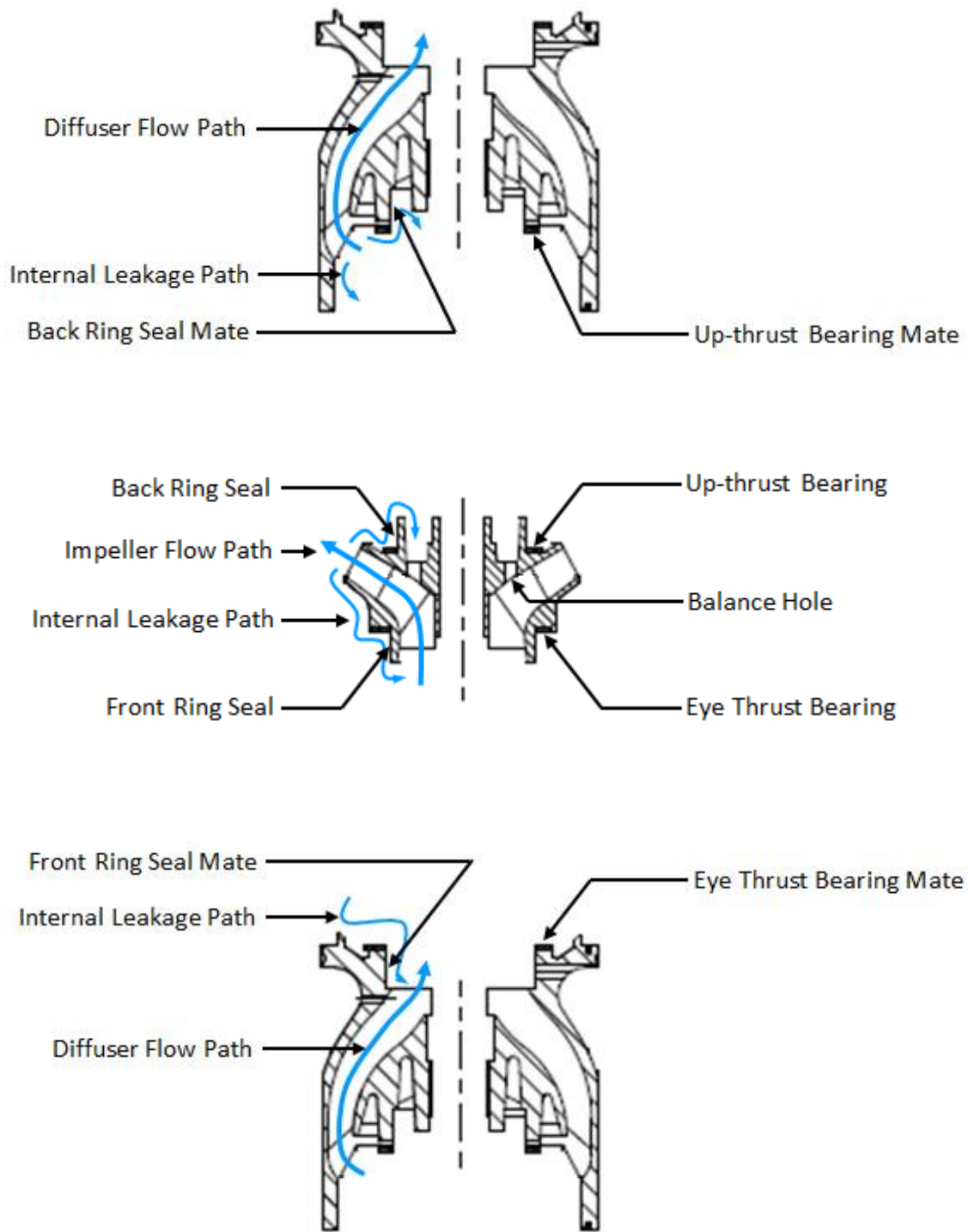
Figure 4. Mixed flow impeller (center) and two diffusers (upper and lower)

Liquid Pump Mechanics

The purpose of each impeller and diffuser is to increase the fluid pressure. The impeller rotates and imparts energy to the fluid in the form of flow, kinetic, internal, and potential energies [9]. These forms of energy manifest themselves as rises in pressure, velocity, temperature, and elevation, respectively. The diffuser decreases the fluid velocity in order to convert excess kinetic energy into flow energy, i.e. to further increase the fluid pressure. The impeller contributes most of the overall pressure rise [10]. The rise in temperature and elevation are generally small. The velocity field and pressure field within a radial flow pump stage are illustrated in Figure 5. The general flow field trends are general to all pumps, including turbine pumps. The pump's inlet is at the center of the annulus and the pump's exit is at the periphery. The velocity field shows that the fluid is accelerated by the impeller and decelerated by the diffuser. This results in the highest velocities at the boundary between the impeller blades and diffuser vanes. The pressure field shows that the fluid is steadily pressurized from inlet to outlet.
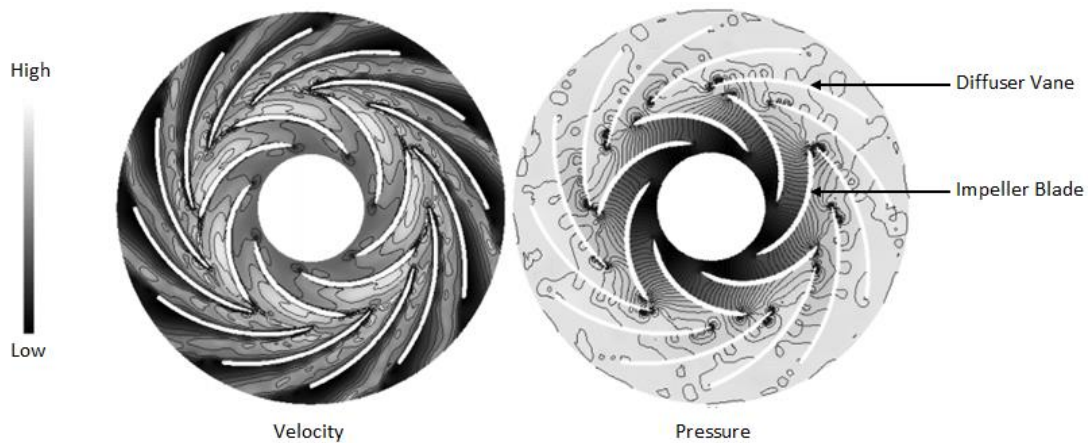
Figure 5. Velocity field (left) and pressure field (right) in a radial flow pump [11]

Liquid-Particulate Pump Wear Mechanisms

Liquid-particulate pump wear has been extensively studied [12]. The primary

mechanisms of liquid-particulate pump wear are abrasion and erosion [13]. The two

mechanisms of wear are depicted in Figure 6. Abrasive wear occurs when particles are

trapped between two surfaces that move relative to one another and erosive wear occurs

when particles impact a surface. Abrasive and erosive wear increase as particle size,

concentration, angularity, relative velocity, and hardness increase and as the surface

hardness decreases (for metallic surfaces). Erosive wear also increases as particle

density and impingement angle α increase.
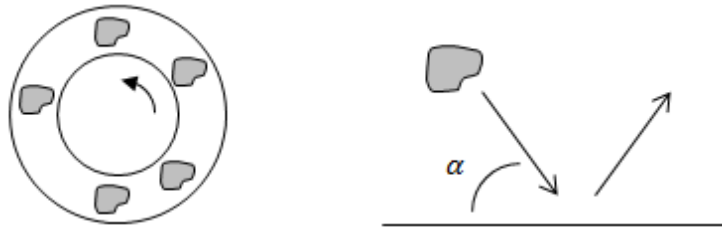
Figure 6. Abrasive (left) and erosive (right) wear

Liquid-Particulate Pump Design

Pumps handling high solid particle concentrations are called slurry pumps and

are specifically designed to minimize wear [13]. Many of the factors that increase pump

wear are independent of the pump design; however, particle impingement angle, particle

relative velocity, and metallic surface hardness can be altered by the pump design to

minimize wear. Particle impingement angles are minimized by selecting geometries that

produce gradually changing fluid pathlines [13]. When fluid pathlines change direction

abruptly, the solid particles do not change their direction as quickly and impinge on

components at large impingement angles, as seen in Figure 7 [14]. This tendency for

solid particles to escape a curved fluid pathline decreases as fluid viscosity increases

[15]. When fluid pathlines do not change abruptly, the solid particles generally follow

the pathlines and therefore impinge at relatively small impingement angles. Most slurry

pumps are radial flow volute pumps with no diffusers, similar to the pump illustrated in

Figure 8 [13]. Unavoidable abrupt changes in fluid pathlines exist at the impeller blade

leading edges and cutwater, as shown in the liquid velocity fields illustrated in Figure 9.

These locations experience significant wear due to particles escaping from the fluid

pathlines.
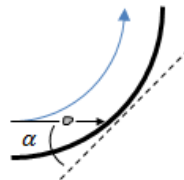
Figure 7. Solid particle escaping curved fluid pathline
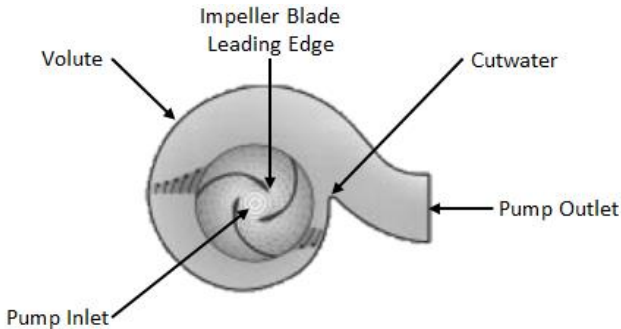
Figure 8. Radial flow volute pump with no diffuser [14]

9
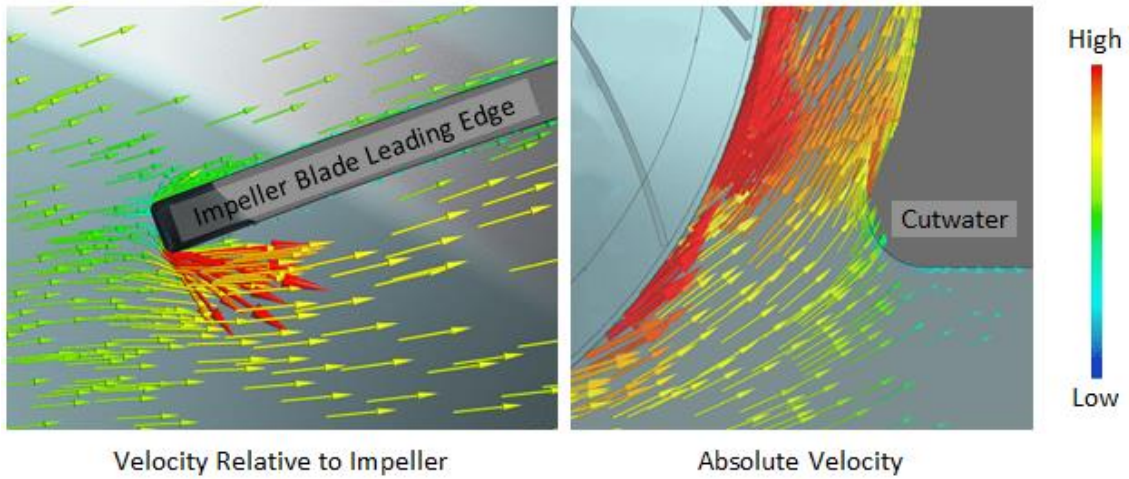
Figure 9. Velocity field at impeller blade leading edge (left) and cutwater (right) [10]

Particle relative velocities are minimized by using low impeller rotational speeds and large cross section flow passages [13]. In order to meet high flow rate requirements, large diameter impellers are also used [13]. High surface hardness is commonly achieved by using abrasion resistant cast irons [13]. Table 2 details three classes of abrasion resistant cast irons found in ASTM A532 [13].

Table 2. ASTM A532 abrasion resistant cast irons [13]

Class	Composition	Hardness (HB)
1	1-11% Cr, 3-7% Ni	500-600
2	11-23% Cr, 0.5-3.5% Mo	600
3	23-28% Cr	400-600

Liquid-Particulate Turbine Pump Wear

Figure 10 shows a detailed depiction of the region identified in Figure 3 on page 4. The impellers are depicted with a black cross section and the diffusers are depicted with a hatched cross section. Turbine pumps are known to experience significant liquid-particulate wear on the areas depicted in Figure 10 [2]. Abrasive wear is the major cause of radial bearing, thrust bearing, and ring seal wear. Erosive wear is the major cause of impeller and diffuser flow path wear. The highest degree of erosive wear generally occurs at the impeller blade leading edge and the diffuser inlet sidewall because large angle impingement occurs at these locations.
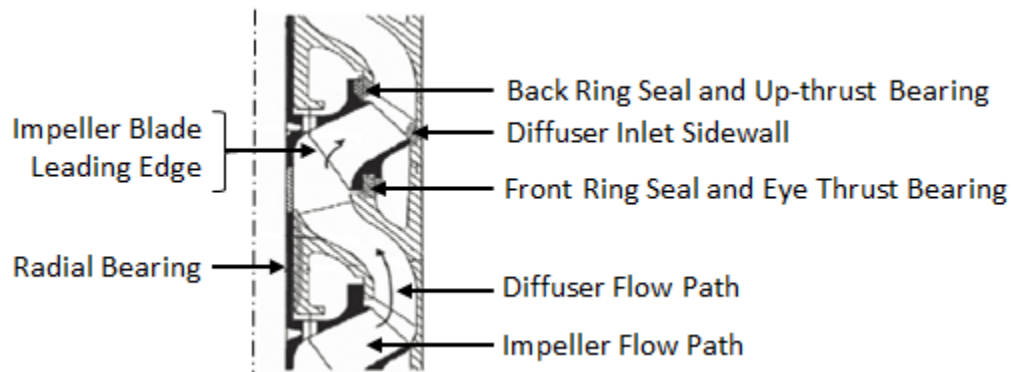
Figure 10. Detail schematic identified in Figure 3 showing areas of significant liquid-particulate erosion in turbine pumps [2]

Liquid-Gas Pump Mechanics

On a detailed level, a centrifugal pump operates by centripetally accelerating fluid particles [16]. The centripetal acceleration acts as a virtual centrifugal force whose magnitude is proportionate to the fluid particle's mass and the applied acceleration. This proportionality has significant ramifications for liquid-gas pumps because a liquid particle has significantly more mass than a gas particle. This large difference in fluid particle mass causes the liquid particles to move much faster than the gas particles. The liquid is able to move the gas by dragging the gas along as the liquid flows past. The difference in fluid particle masses is so extreme that it is appropriate to consider that the impeller moves the liquid and that the liquid moves the gas [17]. This discussion suggests that predominantly gas regions should be dragged radially outward by the liquid. It also suggests that predominantly liquid regions should be located radially outward from predominantly gas regions within a liquid-gas pump. Figure 11 shows the implications of these liquid-gas mechanics in a radial flow impeller. As the figure illustrates, predominantly gas regions form on the pressure side of impeller blade trailing edges, in accordance with the proposed liquid-gas mechanics. The proposed liquid-gas mechanics provide a rough framework from which to qualitatively think about liquid-gas flows. It is important to realize that liquid-gas mechanics are extremely complex and that quantitative treatments, i.e. by Computational Fluid Dynamics (CFD), rely on significant assumptions and are unable to accurately predict liquid-gas behavior without experimental feedback [18].

12

Figure 11. Local GVF field in an impeller supplied by a 17% GVF stream [17]

Liquid-Gas-Particulate Pump Wear

There is anecdotal evidence that adding gas to a liquid-particulate stream increases turbine pump wear [19]; however, the researchers have been unable to find any published literature concerning liquid-gas-particulate pump wear. The remainder of this thesis details an experimental study comparing liquid-particulate turbine pump wear to liquid-gas-particulate turbine pump wear. This study resorted to experimental methods because liquid-gas-particulate wear mechanisms are too complex to be accurately analyzed by CFD techniques [18].

2. METHODOLOGY

This section describes the methodology employed to determine how liquid-gas-particulate turbine pump wear differs from liquid-particulate turbine pump wear. The subsections are as follows:

- Liquid-Gas-Particulate Matter Selected
- Turbine Pumps Selected
- Test Plan

Liquid-Gas-Particulate Matter Selected

Crude oil, natural gas, and sand would be primary candidates for liquid-gas-particulate matter because the goal of the research is related to upstream Oil & Gas ESPs. However, hydrocarbons are difficult to work with because of safety and environmental concerns. Water, air, and sand were chosen because they are safe and readily available in large quantities. Table 3 lists properties of water and air alongside crude oil and natural gas. It is important to note that crude oil is often significantly more viscous than water.

Table 3. Fluid properties at 113 ^{o}F and 14.7 psia [20]

Fluid	Specific Gravity* (--)	Viscosity (10^{-4} Poise)
Water	0.99	60
Crude Oil**	0.87	1300
Air	0.0011	1.94
Natural Gas	0.0006	1.18

* Specific Gravities obtained relative to water at 39 ^{o}F and 14.7 psia
** Crude oil properties obtained from averaging those found in [21]

Table 4 lists properties of the sand used in the experiments. Although the average sand diameter was 4 mils, a dispersion of sizes were actually present. Figure 12 shows the sand size dispersion in terms of a sieve analysis. Any sand retained on or before the 140 mesh sieve had a diameter greater than 4 mils and any sand that passed the 140 mesh sieve had a diameter less than 4 mils.

Table 4. Sand properties

Composition	Specific Gravity* (--)	Hardness (HB)	Mean Diameter (mils)
99.5% SiO_2	2.64	1,300	4

* Specific Gravity obtained relative to water at 39 ^{o}F and 14.7 psia
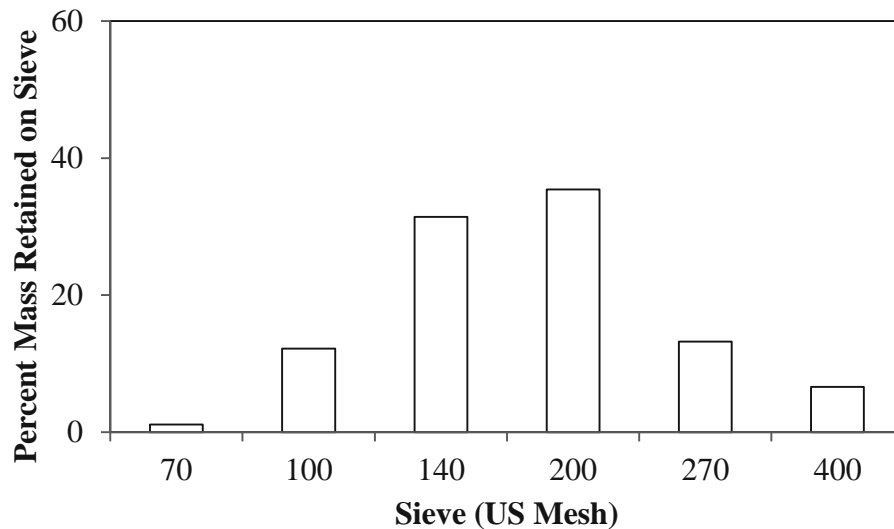
Figure 12. Sand sieve analysis

Given the aforementioned selections, liquid-particulate wear was implemented with Water-Sand, WS, and liquid-gas-particulate wear was implemented with Water-Air-Sand, WAS.

Turbine Pumps Selected

Testing was conducted on two Baker Hughes 1025 MVP G400 Severe Duty turbine pumps. These pumps will be referred to as G400 pumps for the remainder of this document. Each G400 impeller had six blades and each diffuser had seven vanes. One G400 was used for WS testing and the other G400 was used for WAS testing. The G400 pumps have unique gas handling impellers. These impellers allow the pump to handle greater GVFs before experiencing gas lock. Gas lock is the condition when a pump stops flowing due to gas accumulation within the pump [22]. The pumps were selected because a high GVF was desired for the testing and because an alternate goal of the research (not documented in this thesis) was to determine how the unique impeller would wear in comparison to previously tested standard impellers. Figure 13 shows a cutaway view of a turbine pump stage with a standard impeller. The stage consists of one impeller and one diffuser. The direction of flow and impeller rotation is shown in the figure. Diffuser vanes have a pressure side and a suction side. The sides have these names because at any given length along the vane, one side experiences a higher pressure, as illustrated in Figure 5.
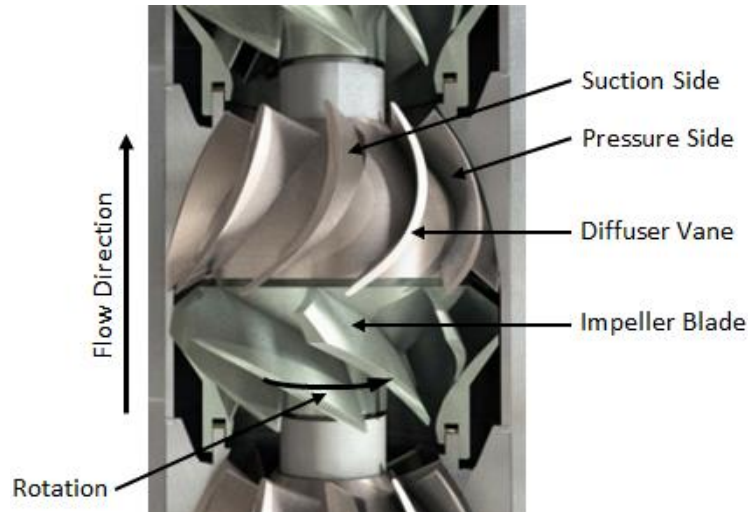
Figure 13. Cutaway view of turbine pump stage with standard impeller [23]

Figure 14 shows a standard impeller. Impeller blades also have a pressure side and a suction side. The pressure side of the impeller blades is the side whose normal roughly points in the direction of rotation and the suction side is the side whose normal roughly points opposite to the direction of rotation. The angle formed between the inlet flow and inlet circumference is known as the blade entrance angle, β_1. The angle formed between the outlet flow and outlet circumference is known as the blade exit angle, β_2. Impeller blades typically have blade exit angles less than 90° because such geometries produce stable power curves [24].

Figure 15 shows the unique gas handling impeller. The gas handling impeller uses split blades, oversized balance holes, and steep blade exit angles [22]. The split blades consist of an inner and outer member. The split blade design encourages mixing between the pressure and suction side of the blades and allows predominantly gas regions to mix with predominantly liquid regions, respectively [22]. The oversized

balance hole design allows internal leakage flow to break up the formation of gas

pockets [22]. The steep blade exit angle design increases the pump efficiency [22]. The

steep blade exit angle also produces a more unstable power curve [24].
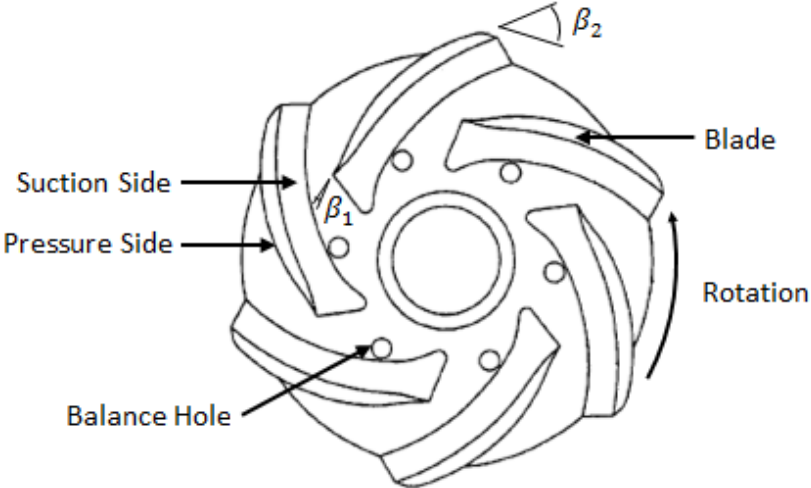
Figure 14. Standard mixed flow impeller [22]
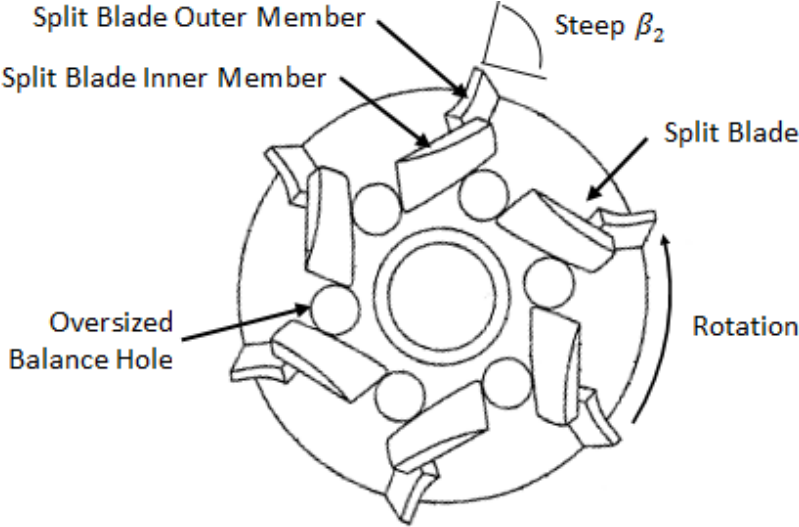
Figure 15. Unique gas handling split blade impeller [22]

Figure 16 displays the manufacturer provided performance curves for each stage of the G400 at 0% GVF. Accordingly, a new G400 stage has a Best Efficiency Point (BEP) at 1,440 gpm and 90 psi. The pump also has a dimensionless specific speed, N_s, of 0.9 at its BEP. Figure 17 displays the required inlet pressure to arrest cavitation for 0% GVF. The inlet pressure curve was determined using Net Positive Suction Head Required ($NPSH_R$) data provided by the manufacturer. Higher GVFs significantly reduce cavitation effects [25]. An inlet pressure of 40 psig is sufficient to minimize cavitation effects provided that 0% GVF flow rates do not exceed 1,300 gpm and temperatures do not exceed 120^oF.
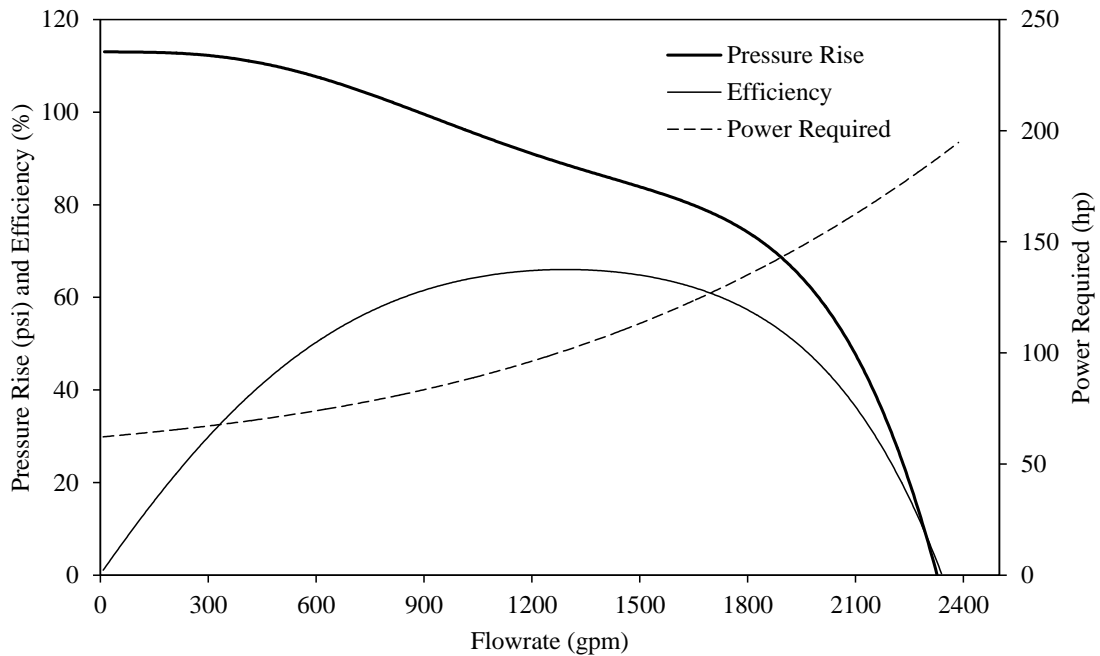
Figure 16. G400 single stage 0% GVF performance curves [26]
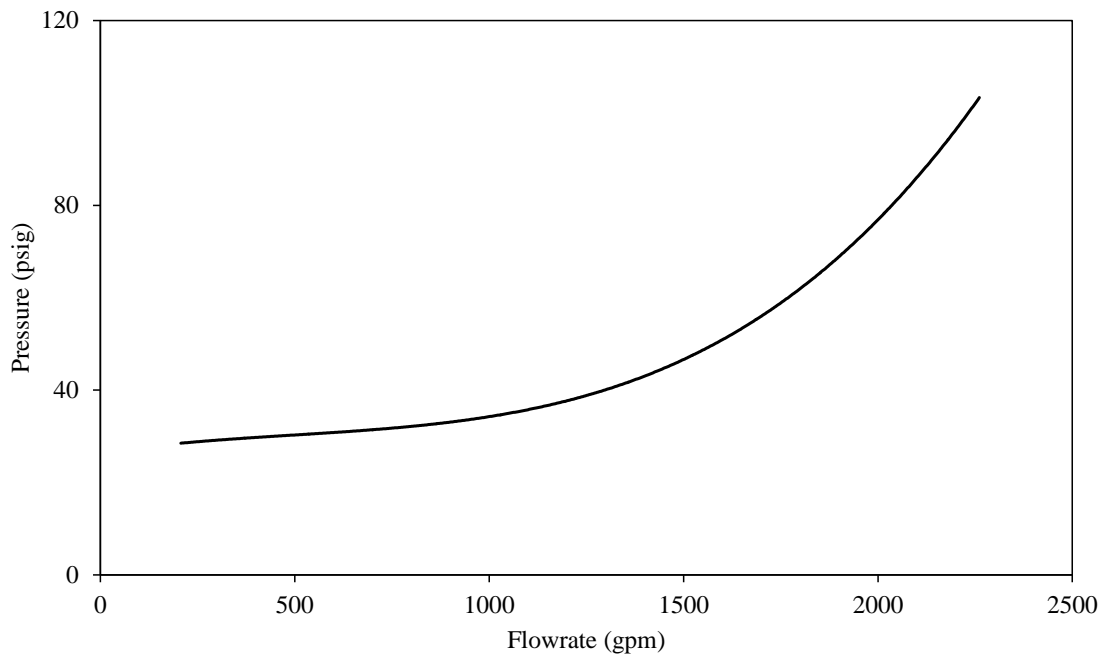
Figure 17. G400 inlet pressure required to arrest cavitation at 0% GVF and temperatures less than or equal to 120°F [26]

Figure 3 on page 4 illustrates the construction of each G400 pump. Figure 4 on page 6 details the other G400 components not listed in Figure 3. Figure 18 and Figure 19 show these components on an actual G400 impeller. Figure 20 through Figure 22 show these components on an actual G400 diffuser. Each radial bearing consists of two parts, an outer bushing and an inner shaft sleeve. Figure 22 shows the outer bushing and Figure 23 shows the inner shaft sleeve. The gap between these parts is referred to as the radial bearing clearance.

20
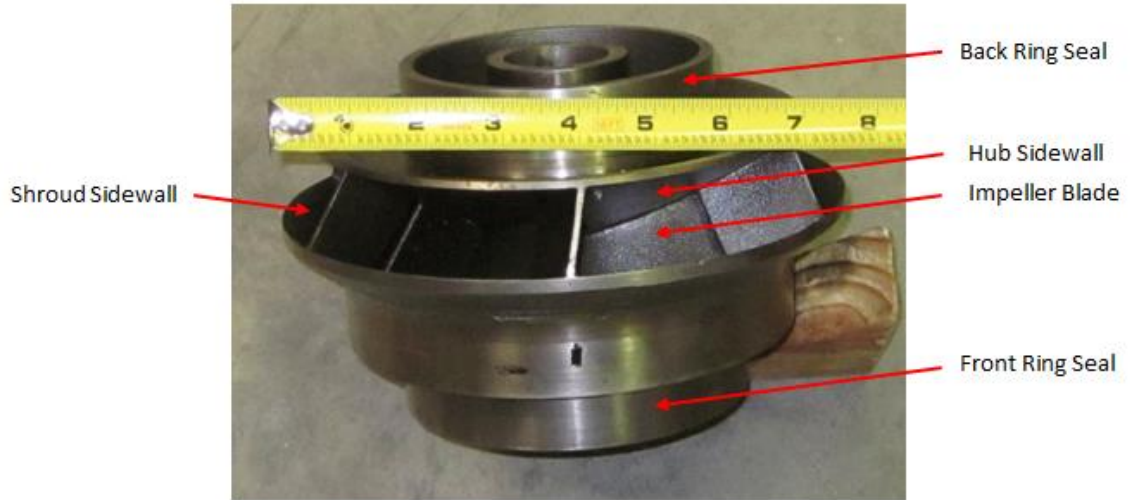
Figure 18. G400 impeller overall view
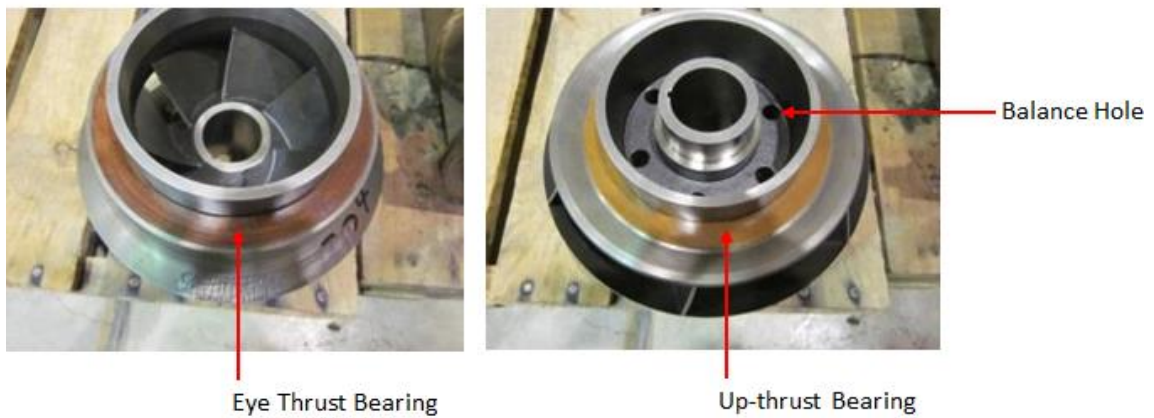
Figure 19. G400 impeller inlet view (left) and exit view (right)

Figure 20. G400 diffuser overall view
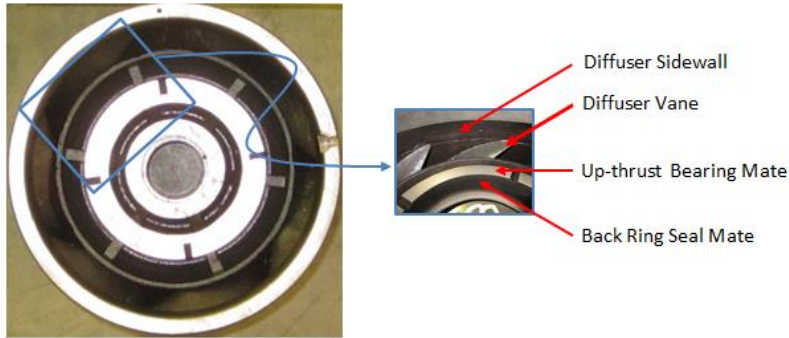
Figure 21. G400 diffuser inlet view (left) and inlet detail view (right)
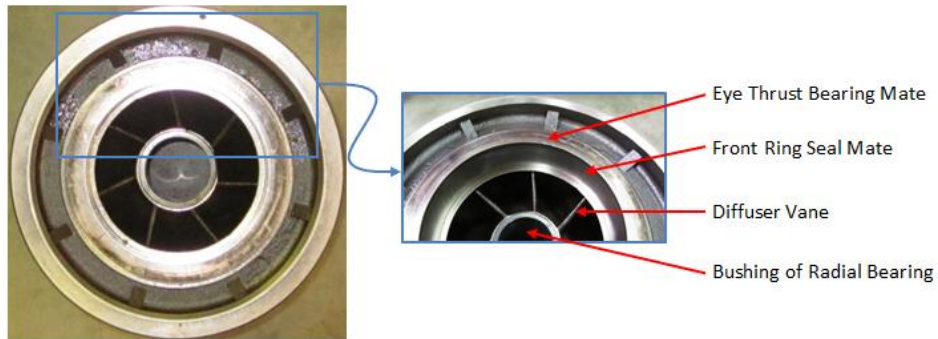
Figure 22. G400 diffuser outlet view (left) and outlet detail view (right)

Figure 23. G400 shaft sleeve of radial bearing

Table 5 details the materials used for all G400 components except the impeller thrust bearings. The impeller thrust bearings were made of a composite; detailed material properties for the composite are unknown to the researchers.

Table 5. G400 component material properties [26] [27]

	Impeller and Diffuser	**Radial Bearing**
Material	Ni-Resist 1b	Cemented Carbide
Composition	13.5-17.5% Ni, 2.5-3.5% Cr, 1.0-2.8% Si, 5.5-7.5% Cu, 0.5-1.5% Mn, 3.0% max C	70-97% WC, 30-3% Co
Hardness (HB)	150-250	1,750

The G400 pump used for WS testing, referred to as the WS G400, had been previously used at a Shell Oil Company testing facility and consisted of two stages. The G400 pump used for WAS testing, referred to as the WAS G400, was new and consisted of three stages. Before wear testing was conducted, 0% GVF performance curves were obtained for both G400 pumps. Figure 24 shows the performance curves for the WS G400 and Figure 25 shows the performance curves for the WAS G400. The WS G400 shows more deviation from the manufacturer provided curves than the WAS G400. This is due to the fact that the WS G400 was previously used. The WS G400 deviation displays classic impeller wear [28].
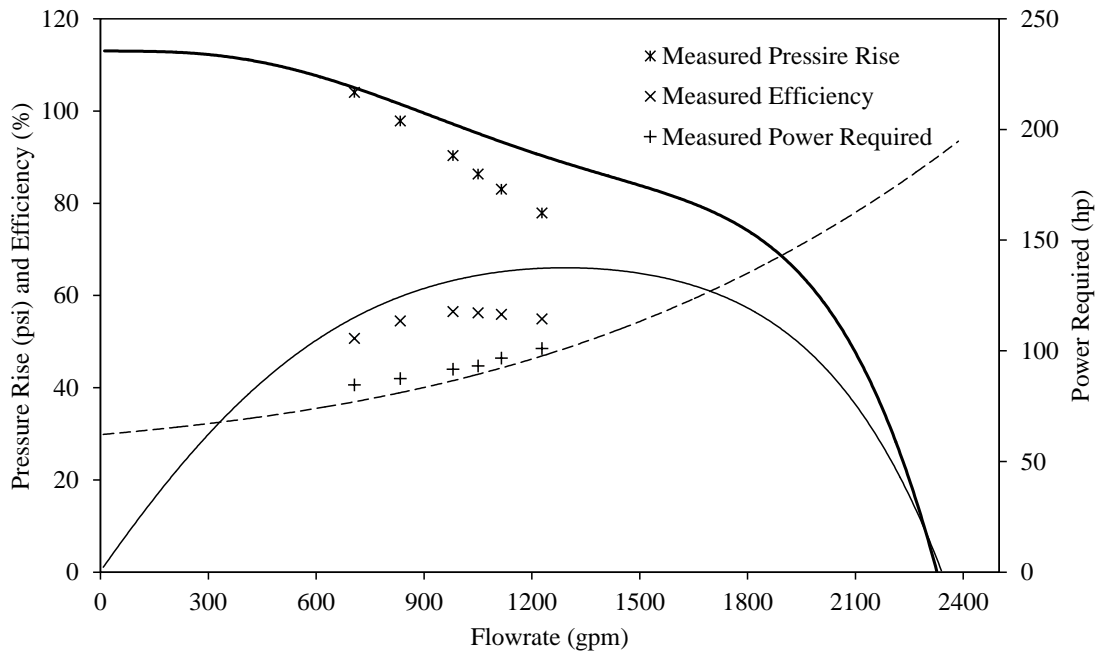
Figure 24. G400 single stage 0% GVF measured performance curves before WS testing
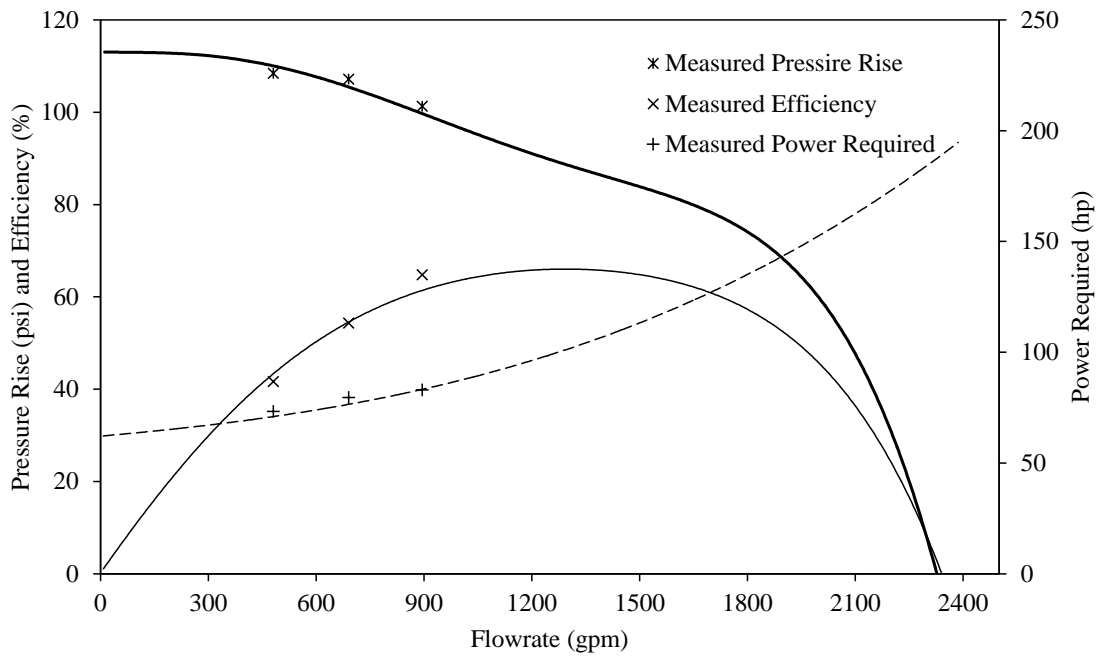
Figure 25. G400 single stage 0% GVF measured performance curves before WAS testing

24

For the WS G400 measurements, the upper flow rate was limited by the smallest possible test loop resistance achievable. For the WAS G400, the upper flow rate was limited by the maximum horsepower the pump's motor could supply (the WAS G400 had one more stage than the WS G400). For both G400s, the lower flow rate was limited by considering the fact that reducing the flow rate increases the temperature rise within the pump and can cause cavitation to begin at lower pressures than predicted (the predictions detailed in Figure 17 on page 20 were based on a 120°F maximum liquid temperature). Although 0% GVF performance curves are hampered by a narrow flow rate range for the WAS G400, 12% GVF performance curves can be obtained for wider flow rate ranges (because GVF reduces power requirements and therefore relax the upper flow rate limitation). In order to evaluate performance changes over the widest possible range of flow rates, performance curves at 12% GVF will be presented in the Results and Discussion section.

Test Plan

A WS wear test was conducted on one G400 pump and a WAS wear test was conducted on the other G400 pump. The WS test was conducted at 0% GVF and the WAS test was conducted at 20% GVF (with respect to, w.r.t, the pump inlet). The pump inlet pressure was maintained at 40 psig. This inlet pressure was selected to arrest cavitation while minimizing test loop construction costs. Each pump was operated at its BEP at the corresponding GVF. Both tests were conducted with a sand concentration of 0.2% (by weight). This sand concentration is ten times higher than the severe sand concentration threshold listed in Table 1. This high sand concentration was selected based on previous testing in the lab that produced observable wear after a 200 hour testing period with such a sand concentration. Testing of each pump was conducted for 66 hours. The testing duration was selected by monitoring the assumed worst case test (the WAS test) and ending the test when performance degradation was significant.

Because of the following reasons, the second stage of each pump was determined to be of primary interest.

1. Water and air are poorly mixed before the first stage (see Figure 28 on page 33); however, the first stage mixes the water and air well before the second stage.
2. GVF values (w.r.t. the inlet of each stage) change through a multistage pump.
3. Each stage is affected by different boundary conditions (such as the presence or absence of a preceding or following stage).

Table 6 details the wear test conditions for the second stage of each G400 pump. The liquid flow rates were selected based on BEP considerations, as discussed

26

previously. The GVF w.r.t. the second stage inlet and sand concentration are also

documented. The 17% GVF corresponds to the average GVF at the second stage inlet

during the WAS test. The GVF actually ranged from 15% to 20% at the second stage

inlet during this test. The variation in GVF was caused by the first stage beginning the

test producing a meager 20 psi and ending the test producing 0 psi. The other stages did

not behave in this manner. The odd performance characteristics of the first stage are

believed to be caused by poor water and air mixing at the pump inlet. This statement

reinforces the need to focus on the second stage. Dimensional measurements of each

stage and performance curves for each pump were obtained before and after each test.

Table 6. Second stage wear test conditions

	WS	WAS
Liquid Flow Rate (gpm)	1,050	950
GVF (% w.r.t. second stage inlet)	0	17
Sand Concentration (% by weight)	0.2	0.2

3. EXPERIMENTAL APPARATUS

A majority of the test loop was designed by Nicolas Carvajal Diaz and Gerald Morrison, Ph.D. [29]. The Piping and Instrumentation Diagrams (P&IDs) for the test loop are presented in Figure 26 through Figure 28. Standard symbols, defined in [30], were used in the P&IDs. Items that do not have standard symbols are labeled in the P&IDs. The remainder of this section will explain the complex test loop required for the experiment.

The separator tank in Figure 26 is filled with water during testing. The hopper in Figure 27 is filled with new sand during testing. The upper and lower inlet lines on Figure 28 are connected to the building's water supply and 100 psig air compressor, respectively. Water from the right hand side of the separator tank, in Figure 26, is drawn from the tank by two lines. The upper line takes 5% of the total water flow rate and the lower line takes the remaining 95% of the total water flow rate. The auger in Figure 27 doses the water in the upper line with new sand. The dose rate is adjusted to the proper level by controlling the auger motor speed with its Variable Frequency Drive (VFD).

The upper line, conveying a water and sand mixture, is then boosted by the upper booster pump. The lower line, conveying only water, is boosted by the lower booster pump. Both lines feed into Figure 28. The water and sand line is metered by a coriolis flow meter that measures mass flow rate and mixture density. The water line is metered by an orifice flow meter that measures volume flow rate. The two lines join before the inlet of the tested turbine pump.

Building air at 100 psig is metered by a turbine flow meter that measures volume flow rate. The pressure and temperature of the air are measured near the turbine flow meter. The air flow rate is adjusted by controlling the open degree of a control valve. The air is mixed with the water and sand at the inlet of the turbine pump. The pressure and temperature at the inlet of the turbine pump are collected to calculate the volume flow rate of air into the turbine pump.

The turbine pump is highly instrumented. Pressure transducers record the pressure rise per stage. Triaxial accelerometers record vibration data for the top and bottom of the turbine pump. Proximity probes at the pump coupling record coupling displacement. An optical keyphasor probe at the coupling also records the turbine pump's speed. Building water is injected into the mechanical seal by a positive displacement pump to protect the seal faces from sand.

The effluent of the pump is throttled by a pinch valve and a restriction orifice before being sent to a bank of cyclone separators in Figure 26. The water must be cycled through the pump because of the large flow rate required. The sand however, cannot be cycled through the pump because it would lose its abrasive qualities if it was cycled. The air does not need to be cycled because it is readily available. The cyclone separators provide the first means of effluent separation. The cyclones separate the effluent into two streams: a water and air stream as well as a water and sand stream. The water and air stream is sent to the left side of the separator tank and the air is allowed to go to the atmosphere. The water and sand stream is dropped onto the trough and subsequently dumped onto the back end of the shaker separator. The shaker separator

consists of an inclined screen and unbalanced motor. The water and sand slowly move down the shaker separator as some of the water drips into the left side of the separator tank. When the sand reaches the end of the shaker separator, it drops into the used sand bin. The used sand is donated to a local recycling company and a new sand bag is used to replenish the hopper.

The left hand side of the separator tank is separated from the right side to allow any sand that may have gotten into the left side of the tank to settle to the bottom. The clean water from the top of the tank spills over into the right side of the tank to replenish it. This cycle repeats continuously during the turbine pump testing. As the water is cycled, the internal energy of the water is constantly increased. A cooling loop illustrated in Figure 26, is used to constantly remove internal energy from the water and maintain a specific water temperature.
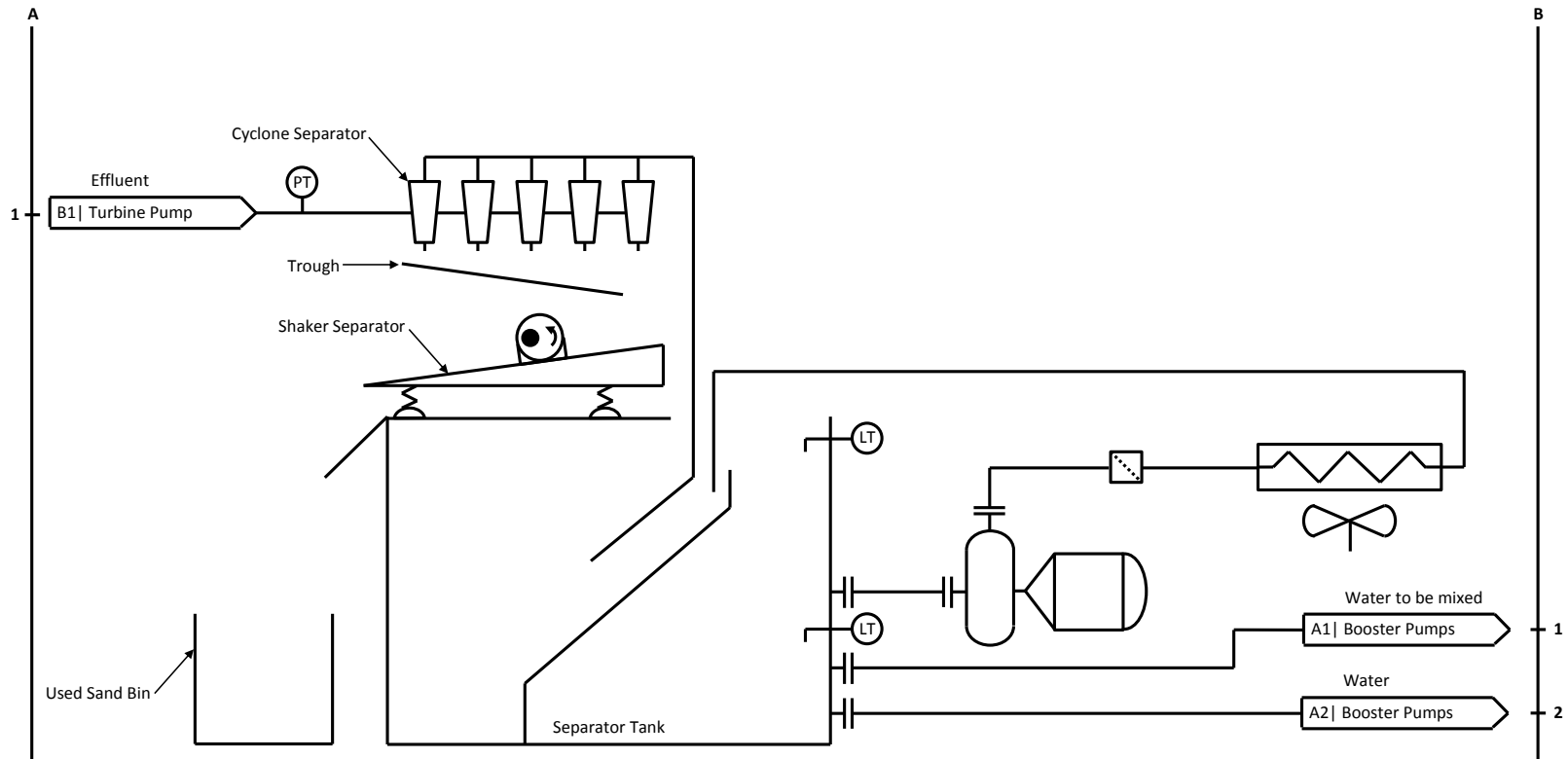
Figure 26. Separator Tank P&ID
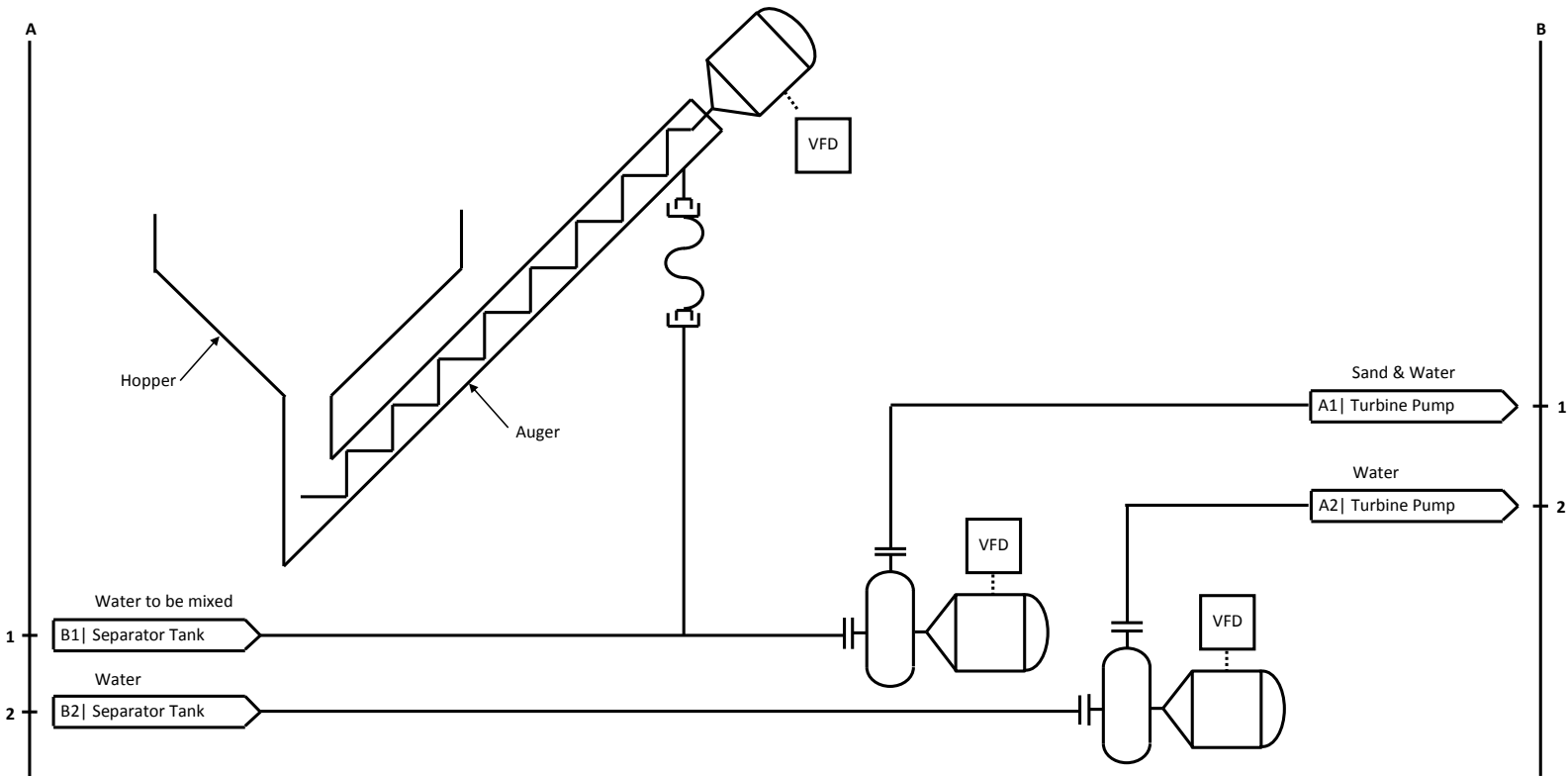
Figure 27. Booster Pumps P&ID
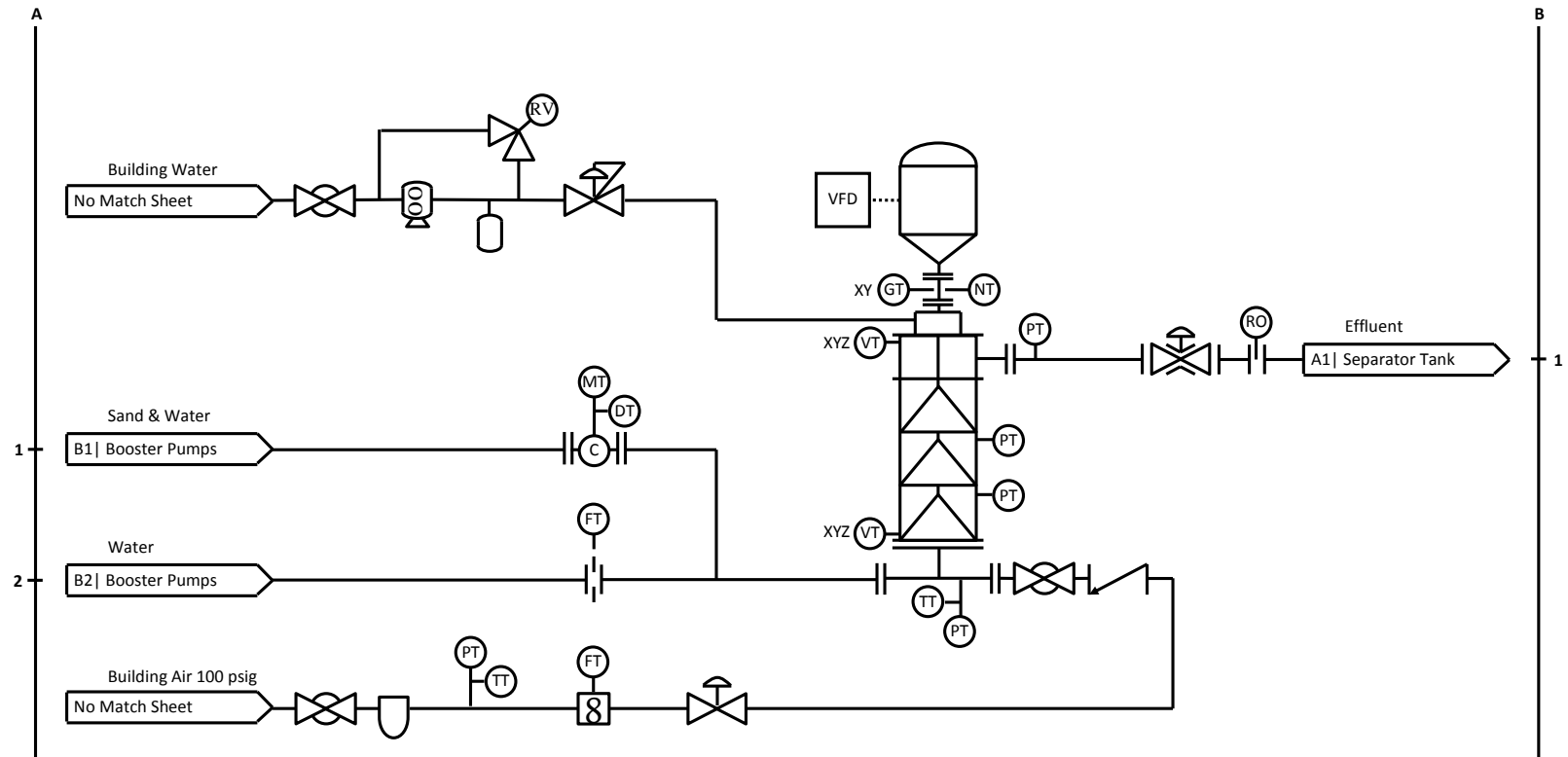
Figure 28. Turbine Pump P&ID

4. RESULTS AND DISCUSSION

This section presents the results of the testing. The subsections are as follow:

- Visual Results
- Performance Results
- Dimensional Measurement Results

Visual Results

This section presents visual results. The subsections are as follow:

- Second Stage
    - Pressure Side Wear
    - Impeller Flow Path Wear
    - Diffuser Flow Path Wear
    - Internal Leakage Path Wear
- Per Stage
    - Impeller Flow Path Wear
    - Diffuser Flow Path Wear

Second Stage

This section visually analyzes the second stage of the WS and WAS tested G400.

The second stage was determined to be of primary interest in the Test Plan subsection

presented in the Methodology section.

Pressure Side Wear

Figure 29 illustrates a general wear trend pertinent to impeller blades and diffuser vanes, jointly referred to as flow elements. The left image shows the suction side of a flow element after being tested and the right image shows the pressure side of the same element. The suction side of the flow element experienced minimal wear. This is evidenced by its original cast appearance. However, the pressure side experienced significant wear. This is evidenced by its grooved appearance. The general trend is that the pressure side of flow elements experiences the most wear. This trend is not caused by the pressure difference between the sides. This is evidenced by the fact that at any given length along the suction side of the element, which corresponds to a different pressure, the wear does not noticeably change. Rather, the trend is caused by flow path geometry that causes particles escaping fluid pathlines (viewed in an inertial reference frame) to impact the pressure side of the elements and not the suction side of the elements.
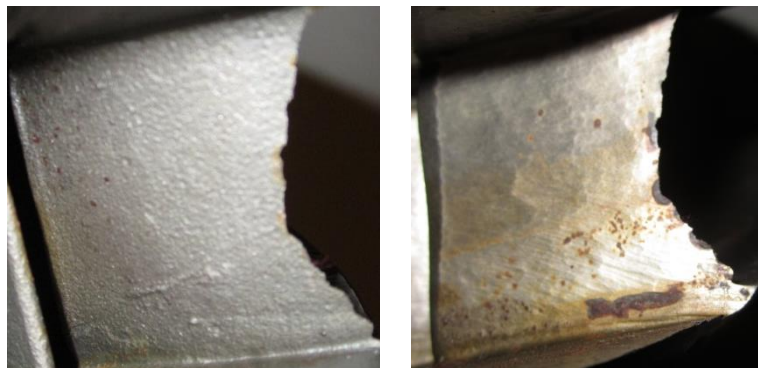
Figure 29. Suction side (left) and pressure side (right) of WAS tested impeller split blade outer member

Impeller Flow Path Wear

Figure 32 shows the G400 second stage impeller before and after the WS and WAS wear tests. The pressure side of the blades experienced a majority of the wear. The leading edges of the split blade inner members for the WS G400 experienced slightly different wear patterns than the WAS G400. The WS leading edges show preferential wear near the mid-span. The WAS leading edges show more uniform wear along the span. The cause of this phenomenon is unknown. Figure 30 shows a close-up view of a split blade outer member before and after WS and WAS wear tests. The leading edge of the split blade outer members for the WS G400 experienced significantly less wear than the WAS G400. Although the leading edges of the inner members were worn similarly, the leading edges of the outer members were worn differently. This difference in leading edge wear behavior is likely due to fluid incidence angle considerations because the larger the discrepancy between fluid incidence angle and blade entrance angle, the greater the wear will be. The inner member and outer member of the G400 split blade both have their own member entrance angle which is analogous to the blade entrance angle for a continuous blade. There was likely a significant discrepancy between inner member entrance angle and fluid incidence angle for both the WS and WAS tests. While there was likely good agreement between outer member entrance angle and fluid incidence angle for the WS test, there was likely a significant discrepancy between outer member entrance angle and fluid incidence angle for the WAS test. It is believed that good agreement between outer member entrance angle and fluid incidence angle for the WS test was produced by uniform flow, with minimal

recirculation zones, within the WS G400 impeller. It is also believed that the significant

discrepancy between outer member entrance angle and fluid incidence angle for the

WAS test was produced by nonuniform flow; with recirculation zones, predominantly

liquid regions, and predominantly gas regions; within the WAS G400 impeller. The

presence of significantly nonuniform flow when gas is present is not surprising because

pumps can be designed to minimize nonuniformities at only one flowrate, pressure rise,

and GVF combination. Furthermore, because liquid-gas flows are not well understood,

it is likely that the G400 pump designers minimized nonuniformities for 0% GVF.

The trailing edges of the split blade outer members for the WS G400 experienced

significantly less wear than the WAS G400. The WS trailing edges were noticeably

worn, but they kept their general geometric shape. The WAS trailing edges were worn

through the thickness of the blade and appear feathered as seen in Figure 30 and Figure

32. Figure 31 shows that the hub sidewall for the WS G400 experienced significantly

less wear than the WAS G400. The shroud sidewalls experienced similar wear. Figure

33 shows a meridonal section of a G400 stage. A meridonal section is obtained by

taking an axial cross section of a stage and then translating flow element geometry to the

cross section. The meridonal section view provides a convenient way to visualize three

dimensional pump flow. Figure 34 maps the unique WAS trailing edge and hub sidewall

wear to the meridonal section. Figure 34 also maps a predominantly air region to the

meridonal section based on liquid-gas pump mechanics presented in the Introduction.

Figure 34 suggests that predominantly air regions increase wear. This suggestion is

substantiated by the fact that air is significantly less viscous than water and lower fluid

viscosity allows particles to more easily escape from fluid pathlines. This phenomenon

was documented in the Liquid-Particulate Pump Design subsection presented in the

Introduction.
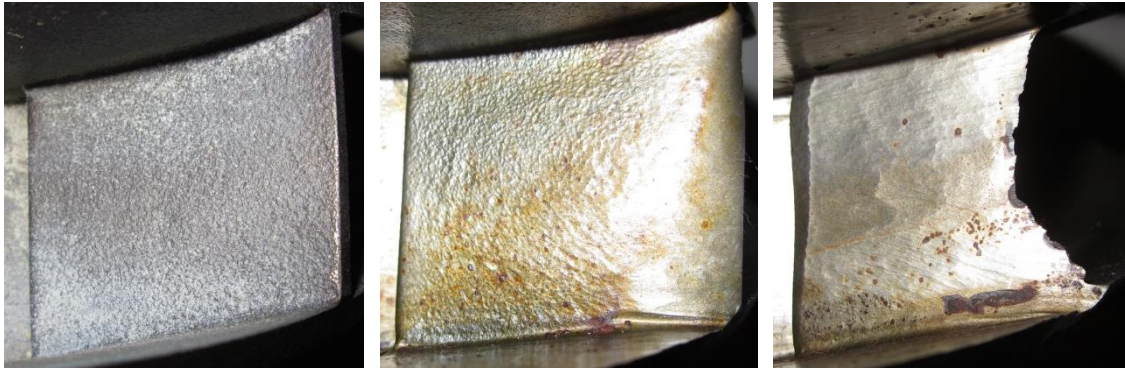
Figure 30.Untested (left), WS tested (middle), and WAS tested (right) second stage split blade outer member

Figure 31.Untested (left), WS tested (middle), and WAS tested (right) second stage hub sidewall

Figure 32. Untested (top), WS tested (middle), and WAS tested (bottom) second stage impeller. Inlet views are displayed on left and outlet views are displayed on right.
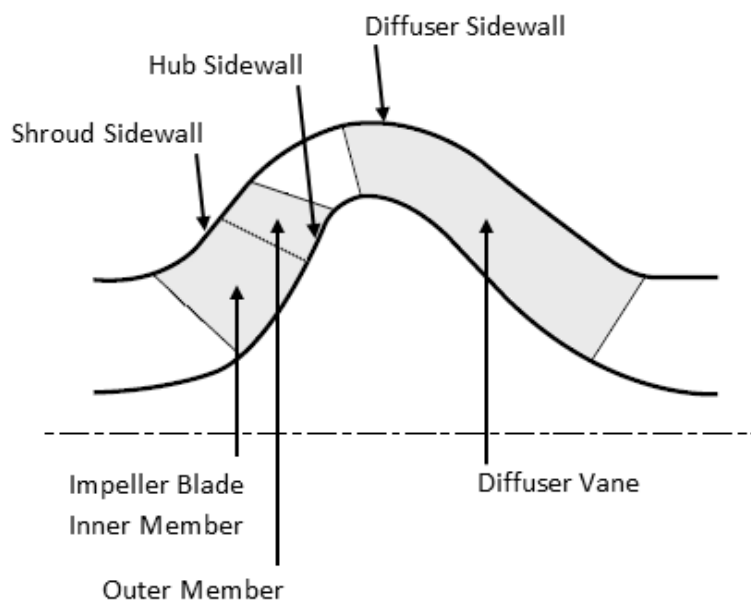
Figure 33. G400 stage meridonal section
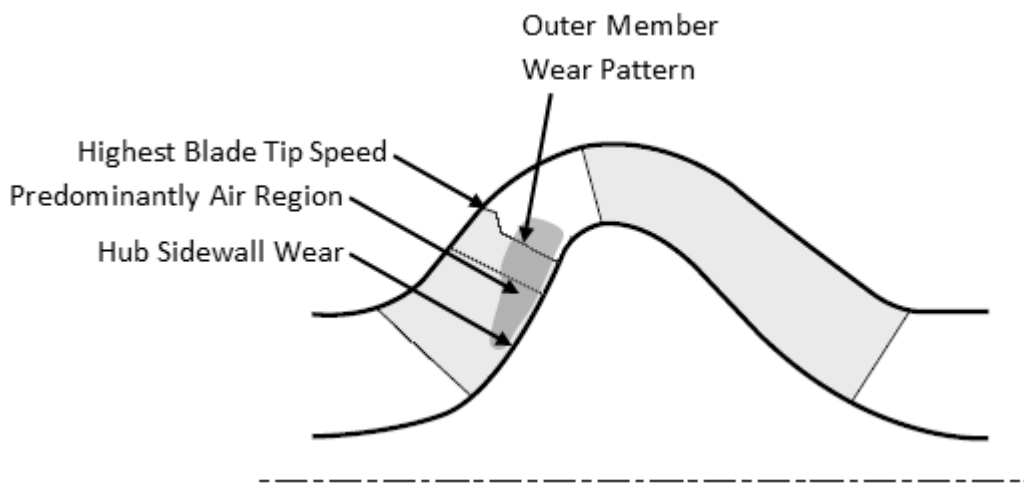
Figure 34. WAS tested meridonal section

40

Diffuser Flow Path Wear

Figure 35 shows the G400 stage diffuser before and after WS and WAS wear tests. In general, the pressure sides of the vanes experienced more wear than the suction sides. However, the suction side of the diffuser vane leading edges did experience significant wear as can be seen in Figure 35. This is simply due to a poor mismatch between diffuser vane entrance angle and fluid incidence angle. This mismatch is caused by poor interaction between the impeller and diffuser. This poor interaction could be explained by the fact that the split blade impeller was designed to be used directly in place of existing impellers and the interaction between the split blade impeller and the existing diffusers may not be rigorously checked by the manufacturer [22]. The leading edges of the diffuser vanes for the WS G400 experienced significantly different wear patterns than the WAS G400. Although the leading edges for both diffuser vanes experienced preferential wear nearest the diffuser sidewall, different wear patterns along the span of the leading edge and extending along the length of the diffuser vanes were present as can be seen in Figure 35. The WS diffuser vanes showed uniform wear near the leading edges. The WAS diffuser vanes showed nonuniform wear near the leading edges. The WS leading edges are less jagged than the WAS leading edges. The WS diffuser vanes near the leading edges also have fewer gouges than the WAS diffuser. The nonuniform wear in the WAS diffuser was likely caused by recirculation zones, predominantly liquid regions, and predominantly gas regions present in the WAS diffuser that were not present in the WS diffuser.

41
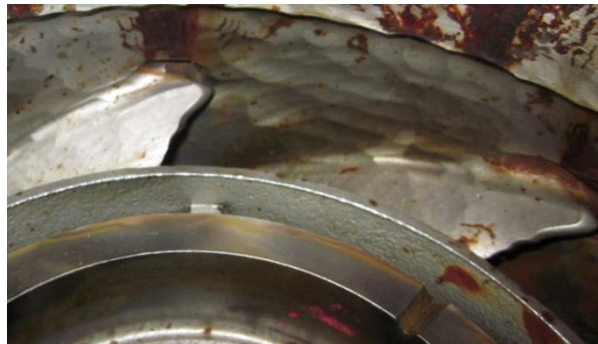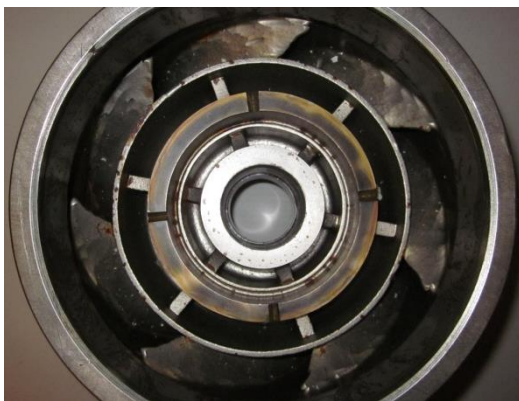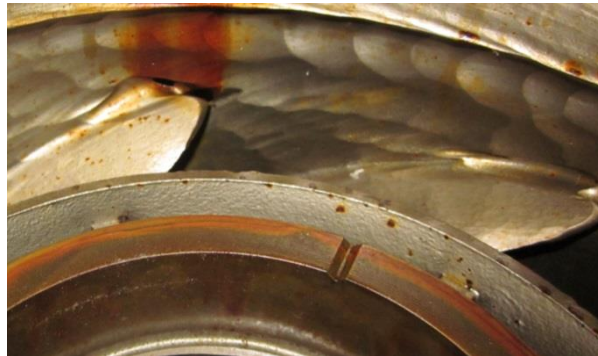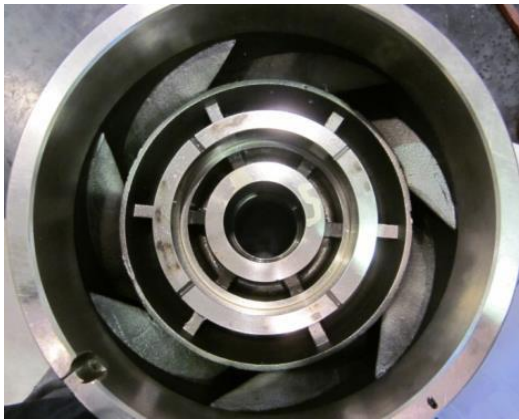
**Figure 35. Untested (top), WS tested (middle), and WAS tested (bottom) second stage diffuser. Inlet views are displayed on left and a close-up inlet view of two diffuser vanes are displayed on right.**

The WS tested and WAS tested diffuser inlet sidewall were severely scalloped as can be seen in Figure 35. The diffuser inlet sidewalls experienced severe wear because fluid pathlines change direction abruptly at the diffuser entrance as seen in Figure 36 and allow particles to impinge on the diffuser sidewall. The intersection of the diffuser vane leading edge and diffuser sidewall experienced the most wear. The WS tested diffuser developed four holes through the sidewall thickness at the aforementioned intersection point. Two such holes are visible in Figure 37. The WAS tested diffuser developed two holes through the sidewall thickness at the intersection point. Although the amount of wear that took place on the WS tested and WAS tested diffusers was similar, more wear appeared to have taken place on the WS tested diffuser than on the WAS tested diffuser. However, the amount of wear seen on the diffusers cannot be entirely related to the presence or absence of air. A more likely explanation for the similarities and differences in wear is related to the distribution of air within the WAS tested G400 and the amount of energy supplied to the particles by the impellers. The similarities between the wear can be attributed to the presence of a predominantly air region at the location depicted in Figure 36 and the presence of a predominantly water region near the diffuser sidewall during the WAS test. This situation would allow the diffuser sidewall to experience similar wear during the WS testing and the WAS testing because the fluid near the diffuser sidewall would have a similar viscosity for both tests. The differences between the wear can be attributed to the amount of energy supplied to the particles by the impellers. For the WS test, the impeller split blade outer members kept their general geometry and constantly supplied a large amount of energy to the particles. For the

WAS test, the impeller split blade outer members were worn through their thickness and accordingly supplied less energy to the particles as the test progressed. The above explanation suggests that both diffusers were being worn at the same rate at the beginning of the testing; however, as the testing progressed, the WAS tested diffuser began to wear slower than the WS tested diffuser.
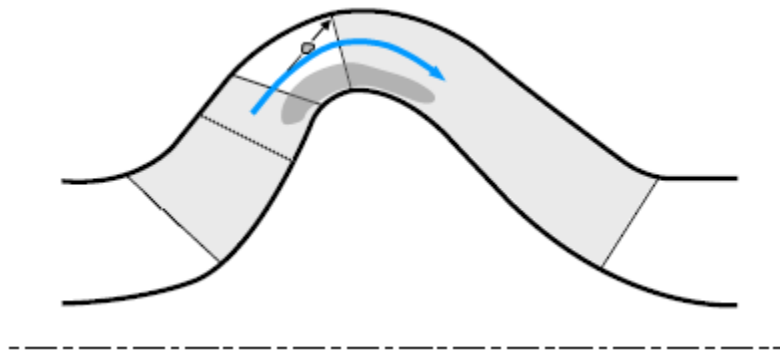
Figure 36. G400 stage meridonal section illustrating a particle escaping a fluid pathline and impacting the diffuser inlet sidewall. A predominantly air region developed within a WAS tested diffuser is also illustrated.

Figure 37. Close-up view of the middle right image in Figure 35. A white cloth was placed behind the diffuser to clearly show two through thickness holes developed at the diffuser vane leading edge and sidewall intersection point.

Internal Leakage Path Wear

Figure 38 identifies points within the WS tested and WAS tested pumps that experienced significant internal leakage wear. Similar internal leakage wear took place for both tests. Deep groves and gouges occurred where internal leakage flow was required to change direction, i.e. at the locations identified in Figure 38. Figure 39 through Figure 42 depict the wear points on the WAS tested G400. The WS tested wear points look similar. Most of the composite thrust bearings were entirely worn away during the tests. The tested pumps were installed in such a way that the thrust bearings would not counteract the thrust generated by the pump, per the manufacturer's instructions. Any thrust generated by the pump was instead taken by the motor's thrust bearings throughout the entire test. The pump would be installed in an oil well in such a way that the thrust bearings would counteract the thrust generated by the pump. Any thrust generated by the pump would initially be taken by the thrust bearings, but would be transferred to the motor as the thrust bearings wore away. This suggests that turbine pump thrust bearing wear could be the root cause of some premature motor failures which one study, summarized in Figure 1 on page 2, found to account for 61% of ESP failures. The small diffuser ribs, seen in Figure 42, were gouged on one side by the internal leakage flow that moved in a downward spiral around the impeller and preferentially wore one side of each rib. Figure 43 shows a radial bearing shaft sleeve before and after erosion. The shaft sleeve is noticeably scratched in the circumferential direction. This wear pattern is common to WS tested and WAS tested shaft sleeves.

(A) Back Ring Seal Mate End Groove
(B) Back Ring Seal Groove
(C) Up-thrust Bearing Wear
(D) Diffuser Lip Groove
(E) Eye Thrust Bearing Wear
(F) Front Ring Seal Groove
(G) Diffuser Rib Gouge
(H) Front Ring Seal Mate Groove
(I) Front Ring Seal Mate End Groove
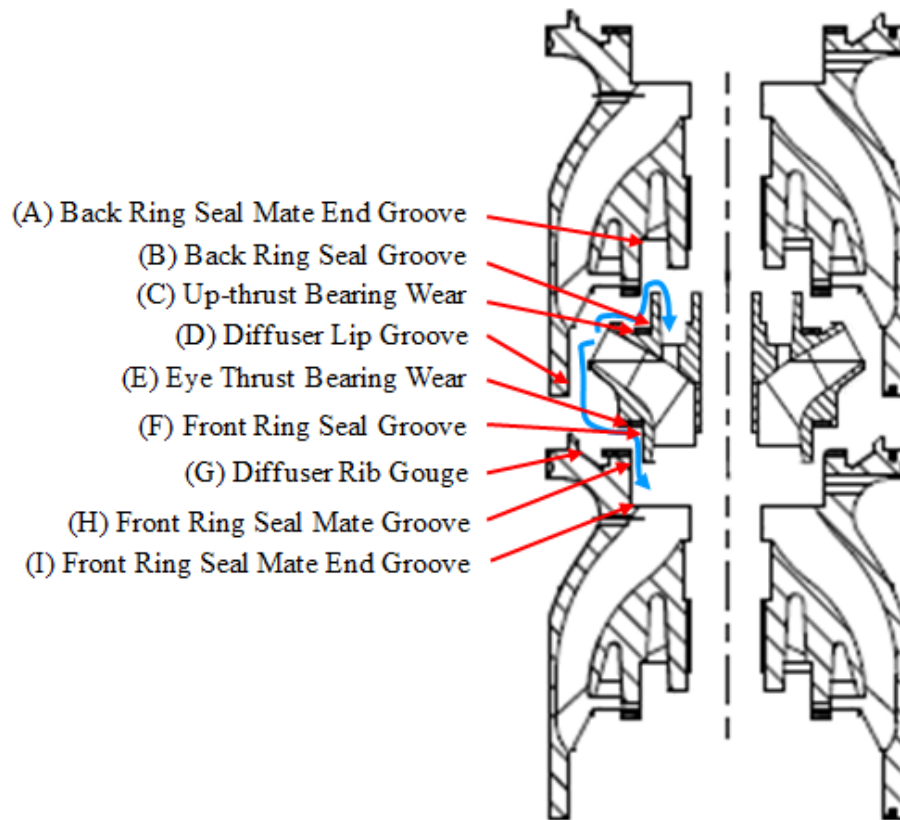
Figure 38. Internal leakage wear points

Figure 39. Untested (left) and WAS tested (right) second stage diffuser inlet. The right image shows the back ring seal mate end groove (A) and diffuser lip groove (D).

Figure 40. Untested (left) and WAS tested (middle and right) second stage impeller outlet. The right image shows the back ring seal groove (B). The middle image shows the worn away up-thrust bearing (C).

Figure 41. Untested (left) and WAS tested (middle and right) second stage impeller inlet. The middle image shows the worn away eye thrust bearing (E). The right image shows the front ring seal groove (F).
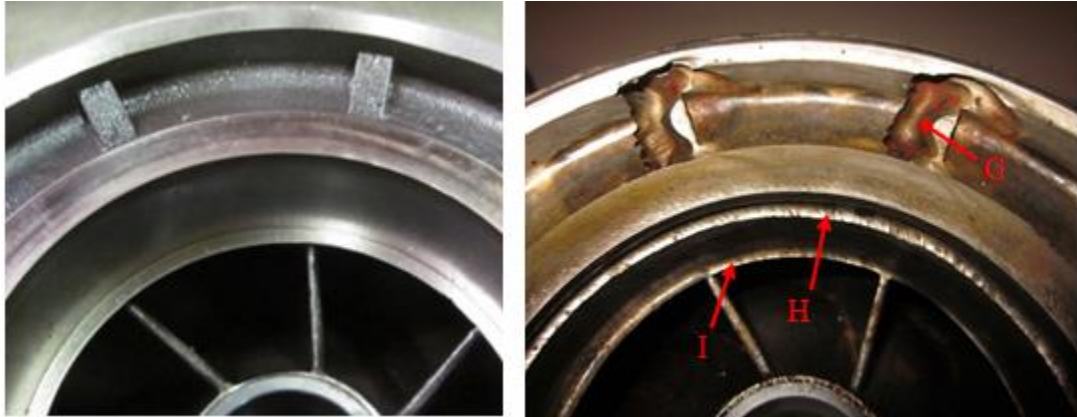
Figure 42. Untested (left) and WAS tested (right) second stage diffuser outlet. The right image shows the diffuser rib gouges (G), the front ring seal mate groove (H), and the front ring seal mate end groove (I).
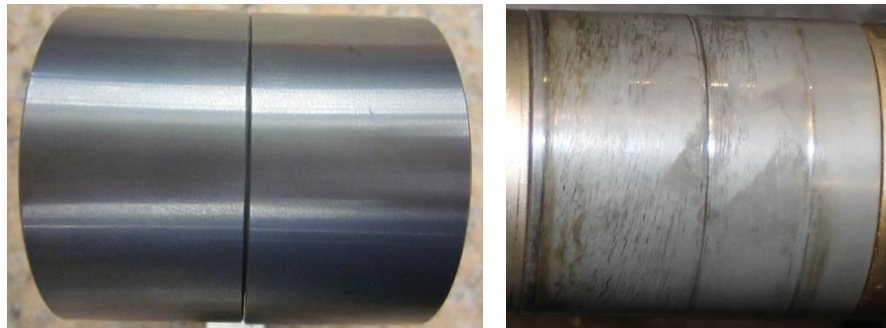
Figure 43. Untested (left) and WS tested (right) radial bearing shaft sleeve

Per Stage

This section visually analyzes each stage of the WS and WAS tested G400.

Impeller Flow Path Wear

Figure 44 shows the WS tested G400 first and second stage impellers. Both stages displayed similar wear, the details of which have already been discussed in the Second Stage Visual Results subsection.

Figure 45 shows the WAS tested G400 first, second, and third stage impellers. The three stages displayed different wear. It is likely that each stage wore differently because each stage had a different inlet pressure and therefore a different inlet GVF. The stage inlet GVF decreased through the pump. The leading edges of the split blade inner members experienced different wear patterns. The first stage leading edges experienced preferential wear near the shroud sidewall. The second stage leading edges showed relatively uniform wear along the span. The third stage leading edges showed preferential wear at the mid-span. The reason for these different wear patterns is unknown, but it is likely that the cause is due to the distribution of air at the inlet of each impeller. The leading edges of the split blade outer members also experienced different wear patterns. The first stage leading edges showed extremely preferential wear near the hub sidewall. The third stage leading edges showed minimal wear similar to that of the split blade outer member leading edges for the WS tests. The second stage leading edges showed moderately preferential wear near the hub sidewall. These observations support the placement of the predominantly air region in Figure 34.

49

Figure 44. WS tested first stage (top) and second stage (bottom) impeller. Inlet views are displayed on left and outlet views are displayed on right.

Figure 45. WAS tested first stage (top), second stage (middle), and third stage (bottom) impeller. Inlet views are displayed on left and outlet views are displayed on right.

Diffuser Flow Path Wear

Figure 46 shows the WS tested G400 first and second stage diffusers. The second stage shows more diffuser sidewall wear than the first stage. The second stage developed four through thickness holes in the diffuser sidewall while the first stage developed only one. It is believed that the second stage sidewall wore more than the first stage sidewall because the concentration of solid particles along the sidewall increases through the pump, i.e. the rotating pump flow causes solid particles to migrate radially outward through the pump.

Figure 47 shows the WAS tested G400 first, second, and third stages. The diffuser sidewall wear increased through the pump. The third stage developed five through thickness holes in the diffuser sidewall while the second stage developed two and the first stage developed none. It is believed that the increase in diffuser sidewall wear through the pump was primarily caused by the amount of impeller split blade outer member trailing edge wear as discussed in the Second Stage Diffuser Flow Path Wear subsection.

Figure 46. WS tested first stage (left) and second stage (right) diffuser. Side views are displayed at top, inlet views are displayed in middle and a close-up inlet view of two diffuser vanes is displayed on bottom.
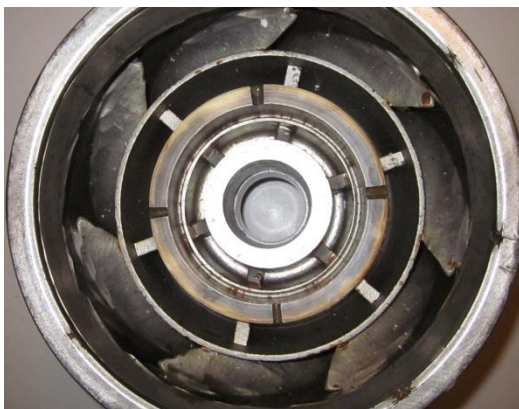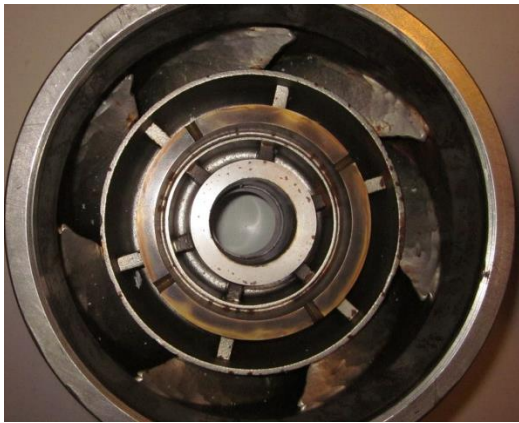
Figure 47. WAS tested first stage (top), second stage (middle), and third stage (bottom) diffuser. Inlet views are displayed on left and a close-up inlet view of two diffuser vanes are displayed on right.

Performance Results

This section presents performance results. The subsections are as follow:

- Test Condition Per Stage Pressure Rise
- 12% GVF Pump Performance and Second Stage Pressure Rise
- 12% GVF Per Stage Pressure Rise

Test Condition Per Stage Pressure Rise

Figure 48 shows the pressure rise produced by the WS G400 stages during the test. The two WS G400 stages began the test producing similar pressure rises, as expected for 0% GVF flow. The first stage showed a slight pressure increase during the test. The second stage showed a slight pressure degradation. This phenomenon will be further discussed in the 12% GVF Per Stage Pressure Rise subsection.

Figure 49 shows the pressure rise produced by the WAS G400 stages during the test. The three WAS G400 stages began the test producing different pressure rises. The stages produced different pressure rises because each stage experienced a different inlet pressure and inlet GVF, as seen in Table 7, and a stage's pressure rise increases with increasing inlet pressure and decreases with increasing inlet GVF. Furthermore, the first stage produced a particularly low pressure rise at the beginning of the test because water and air were poorly mixed before the first stage. Pressure rise data from the middle of the testing period for the first and second stage is missing due to a pressure transducer being plugged with sand. The WAS tested stages showed significant pressure degradation during the test. Table 8 summarizes the pressure degradation for each stage during the WAS test. The first stage showed the most severe pressure degradation. The third stage showed the least severe pressure degradation. The second stage showed a

pressure degradation in between that shown for the first and third stage. The pressure

degradation decreased through the WAS tested pump. The pressure degradation for each

stage has two causes. One cause is the wear of the stage in question. The other cause is

the wear of previous stages that reduces the inlet pressure and increases the inlet GVF

for the stage in question. The stage inlet pressure and GVF at the beginning and end of

the test are detailed in Table 7. The visual results showed that the first stage experienced

severe wear, the third stage experienced minimal wear, and the second stage experienced

wear between that of the first and third stage. The third stage experienced a significant

change in inlet pressure and GVF during the test, as seen in Table 7, but only a minimal

pressure degradation. Because the visual results closely match the pressure degradation

results and the third stage showed minimal pressure degradation even though it

experienced a significant change in inlet pressure and GVF, the pressure degradation for

each stage was dominated by the wear of the stage in question.

Table 7. WAS G400 stage inlet pressure and GVF at the beginning and end of test

Stage	Beginning		Ending	
	Inlet Pressure (psig)	GVF (%)	Inlet Pressure (psig)	GVF (%)
First	40	20	40	20
Second	65	15	40	20
Third	140	8	65	15

**Table 8. WAS test pressure degradation per stage after wear
(data obtained at 20% GVF)**

Stage	Pressure Degradation (%)
First	100
Second	61
Third	16
Overall Pump	43
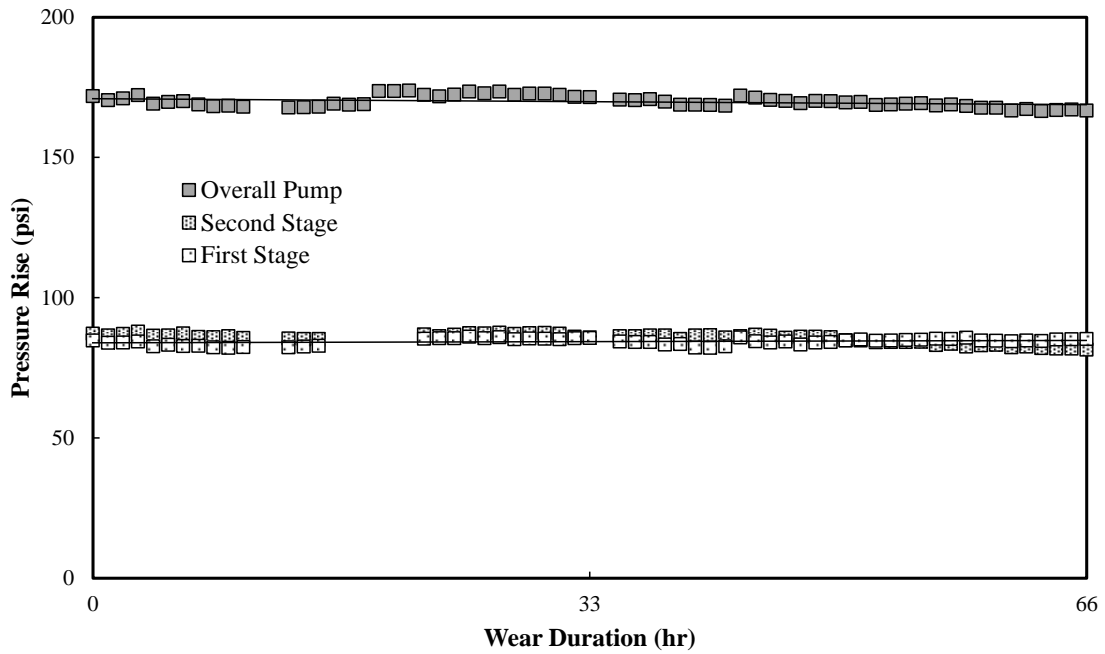
**Figure 48. Pressure degradation during Water-Sand, WS, wear
(data obtained at 0% GVF)**
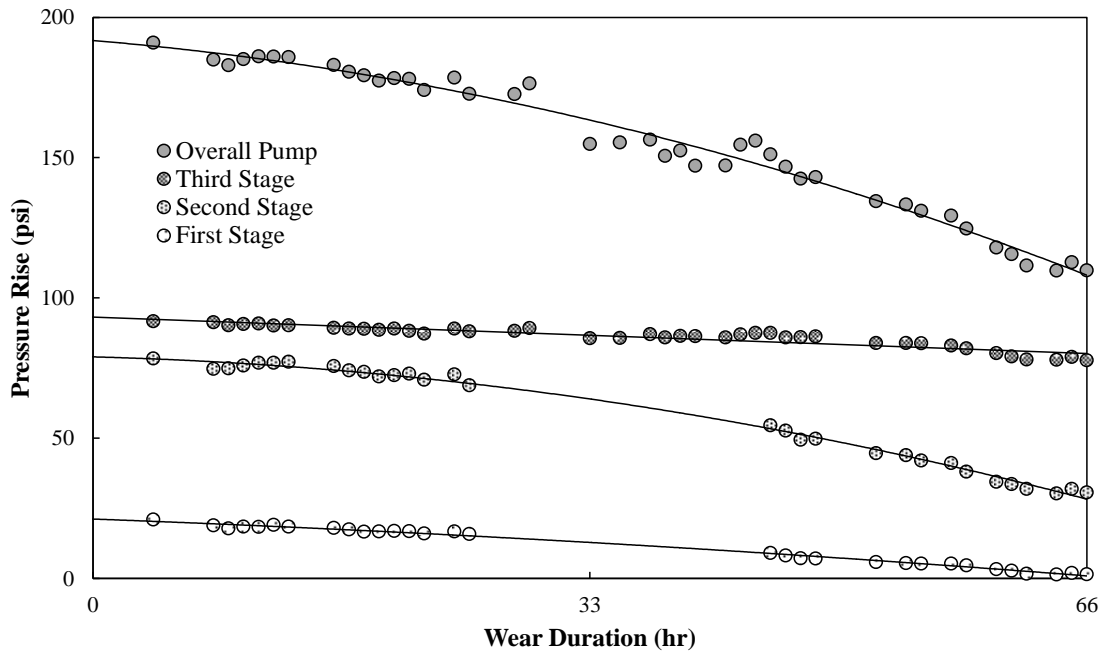
**Figure 49. Pressure degradation during Water-Air-Sand, WAS, wear
(data obtained at 20% GVF)**

12% GVF Pump Performance and Second Stage Pressure Rise

Figure 50 through Figure 55 show power required, efficiency, and pressure rise curves at 12% GVF for each wear test. Performance data for the overall pumps are presented. Although the second stage is of primary interest, power required and efficiency data were only obtainable for the entire pump. Although pressure rise data for the full pump are presented in Figure 54 and Figure 55, the pressure rise for the second stage are more significant and are presented in Figure 56 and Figure 57. Each figure shows how a performance curve changed after the wear test. All performance data is relative to the initial data obtained for each pump because one pump was used while the other was new. Table 9 summarizes the changes in power required, efficiency, and pressure rise. The summary values were obtained by finding the area between the before wear and after wear curves. The WS wear test slightly increased the power required, but the WAS wear test drastically decreased the power requirement. The slight increase in power required during the WS test was likely due to ring seal wear that increased internal leakage. The increase in internal leakage caused the WS tested pump to require more power to maintain the same test condition liquid flow rate. The drastic decrease in power required during the WAS test was caused by the split blade outer members wearing away. The split blade outer member through thickness wear reduced the amount of energy the impellers could impart to the fluid. The WS wear test and WAS wear test produced similar efficiency degradations. This similar efficiency degradation between the WS and WAS test was likely caused by the similar ring seal and radial bearing wear between the two tests. The WAS wear test caused more pressure

degradation than the WS wear test. This is true when looking at the pump's average pressure degradation and at the second stage's pressure degradation. The pressure degradation is primarily associated with the split blade outer member through thickness wear.

Table 9. Wear test pump average performance degradation
(data obtained at 12% GVF)

Wear Type	Power Requirement Increase (%)	Efficiency Degradation (%)	Pressure Degradation (%)
Water-Sand, WS	0.9	3.2	1.7
Water-Air-Sand, WAS	-16.1	3.6	19.6
Increase from WS to WAS	-17.0	0.4	17.9

Table 10. Second stage average pressure degradation after wear
(data obtained at 12% GVF)

Wear Type	Pressure Degradation (%)
Water-Sand, WS	6.2
Water-Air-Sand, WAS	24.5
Increase from WS to WAS (%)	18.3
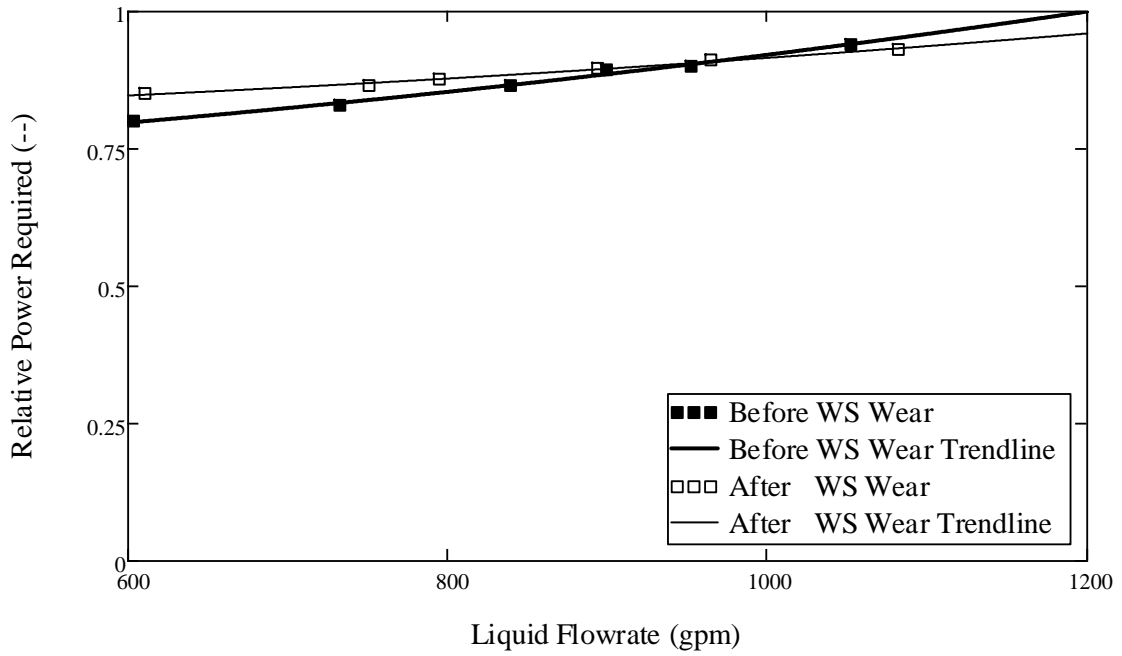
**Figure 50. WS wear test pump power requirement increase
(data obtained at 12% GVF)**
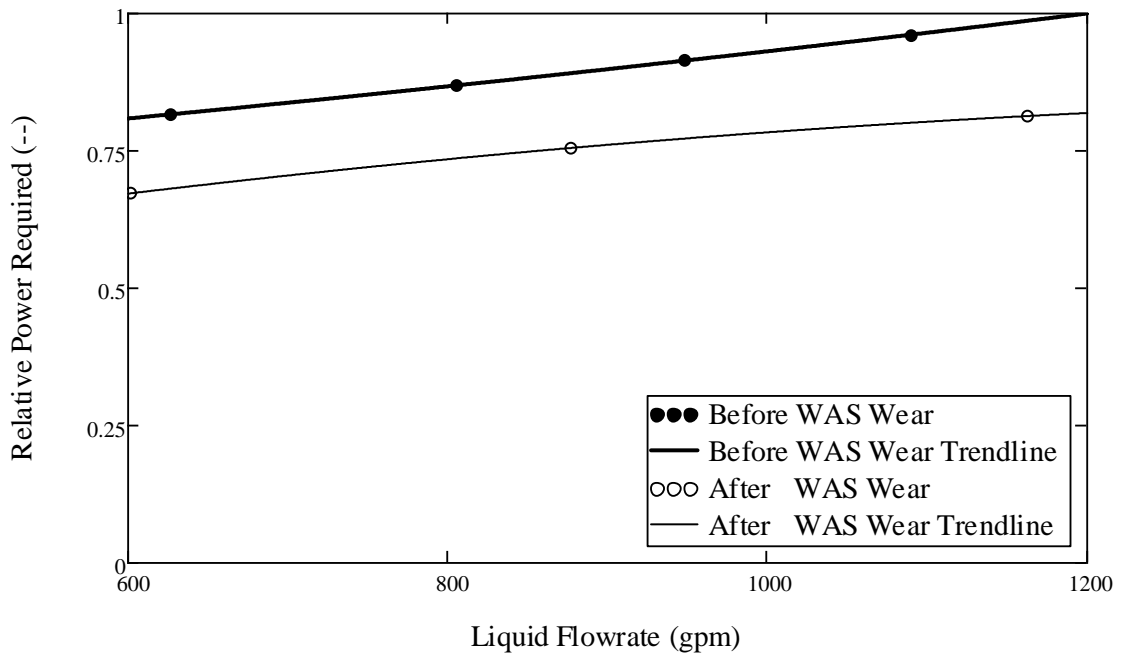
**Figure 51. WAS wear test pump power requirement decrease
(data obtained at 12% GVF)**

61
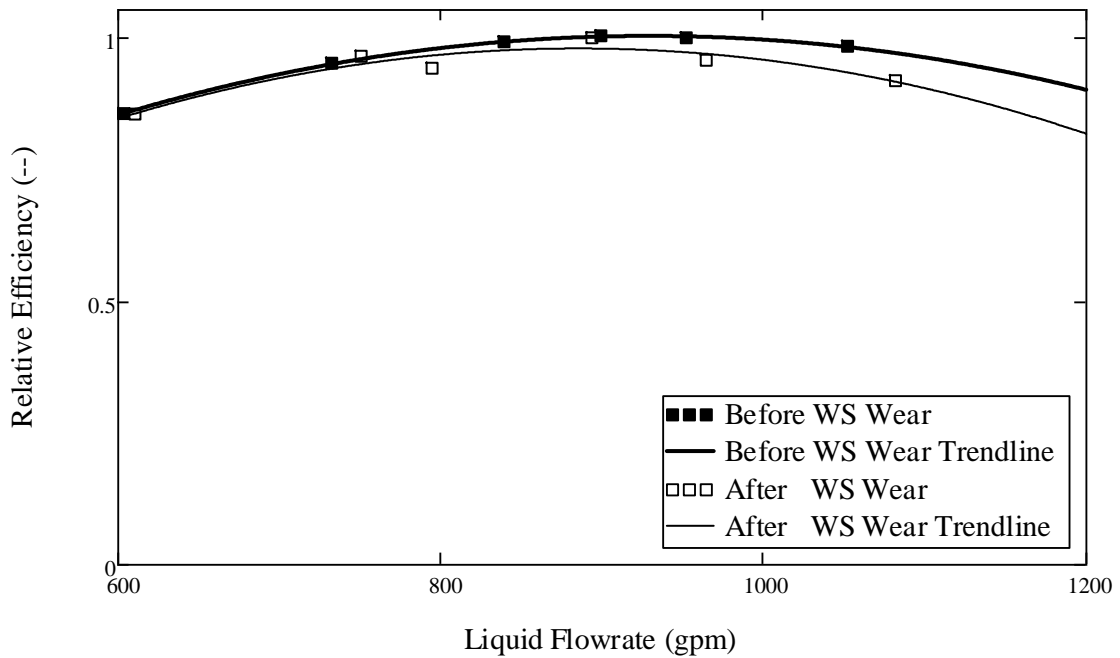
Figure 52. Pump efficiency degradation after Water-Sand, WS, wear (data obtained at 12% GVF)
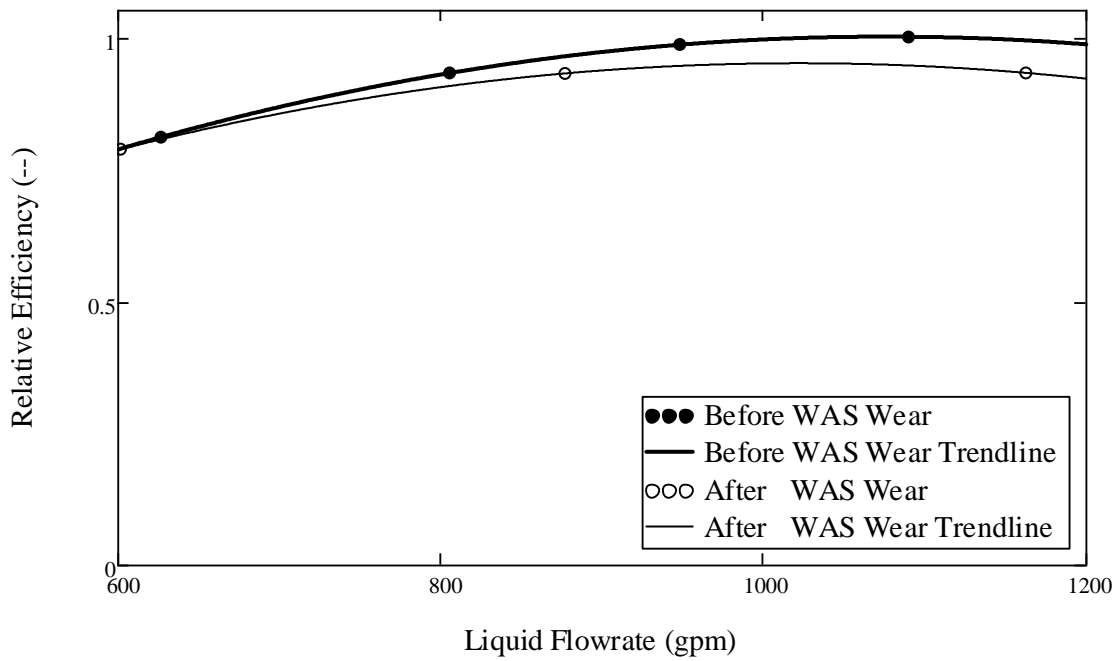
Figure 53. Pump efficiency degradation after Water-Air-Sand, WAS, wear (data obtained at 12% GVF)

62
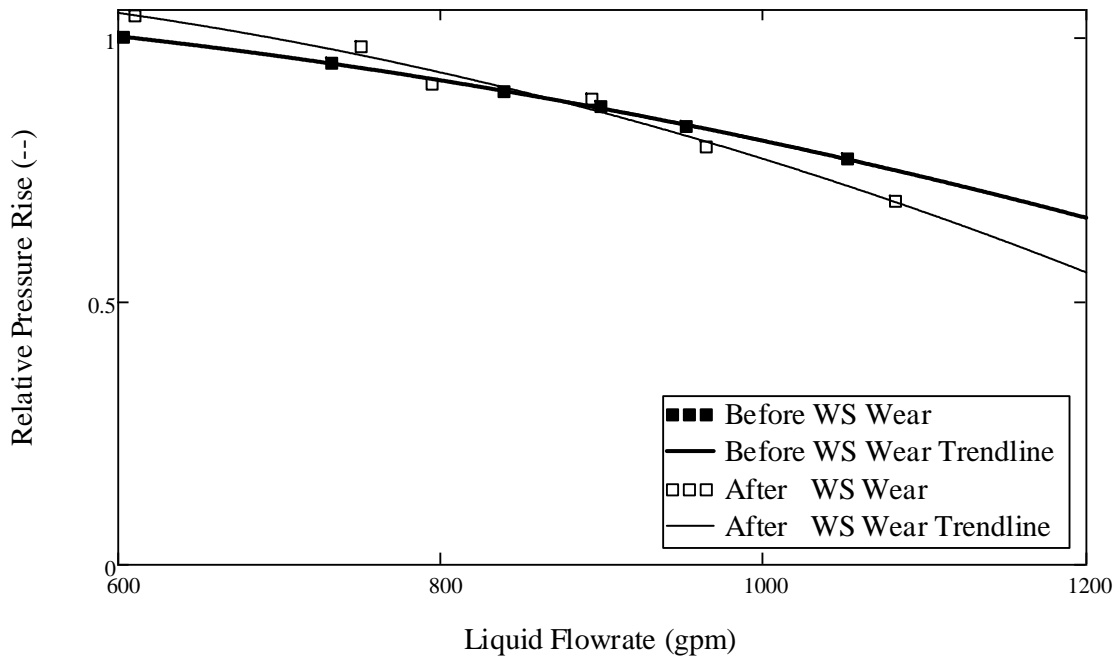
Figure 54. Pump pressure degradation after Water-Sand, WS, wear (data obtained at 12% GVF)
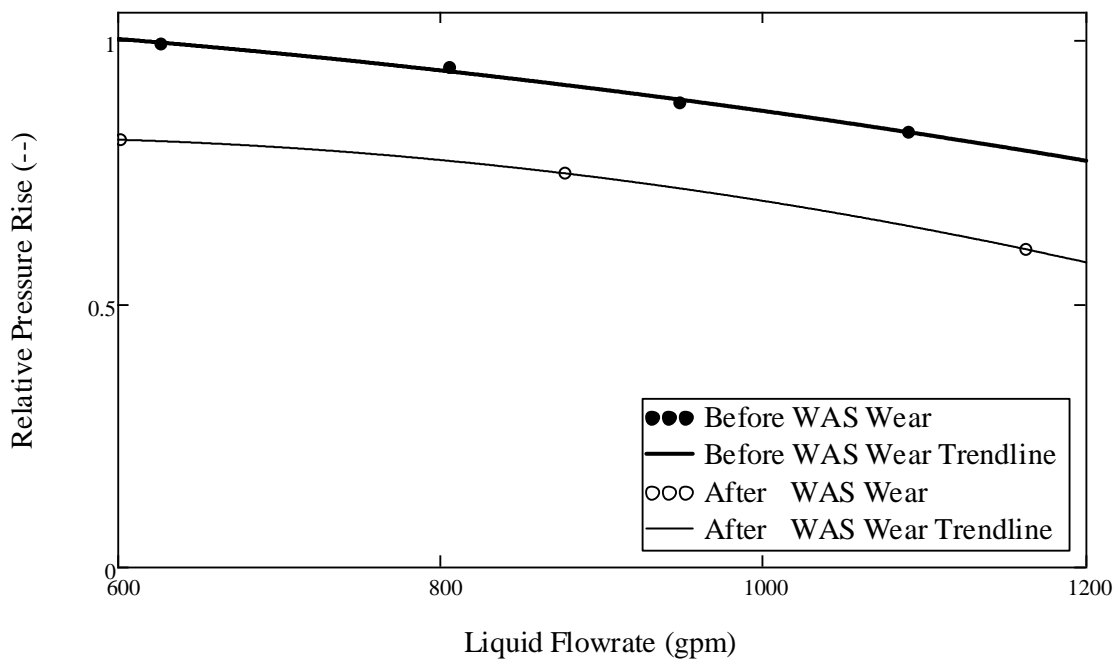
Figure 55. Pump pressure degradation after Water-Air-Sand, WAS, wear (data obtained at 12% GVF)

Figure 56. Second stage pressure degradation after Water-Sand, WS, wear (data obtained at 12% GVF)

Figure 57. Second stage pressure degradation after Water-Air-Sand, WAS, wear (data obtained at 12% GVF)

12% GVF Per Stage Pressure Rise

Figure 58 and Figure 59 show WS G400 pressure rise curves before and after testing for the first and second stage, respectively. Table 11 summarizes the figures. The first stage showed a slight increase in pressure rise; however, the second stage showed a slight decrease in pressure rise. The experimental apparatus, shown in Figure 28 on page 33, has a tee at the pump inlet. The tee produces an undesirable first stage inlet condition. It is possible that the first stage showed an increase in pressure rise because the impeller conformed to the inlet condition. The second stage showed a slight decrease in pressure rise due to ring seal wear.

Table 11. WS test average pressure degradation per stage after wear (data obtained at 12% GVF)

Stage	Wear GVF (% w.r.t. stage inlet)	Pressure Degradation (%)
First	0	-6.0
Second	0	6.2

**Figure 58. First stage pressure change after Water-Sand, WS, wear
(data obtained at 12% GVF)**

**Figure 59. Second stage pressure degradation after Water-Sand, WS, wear
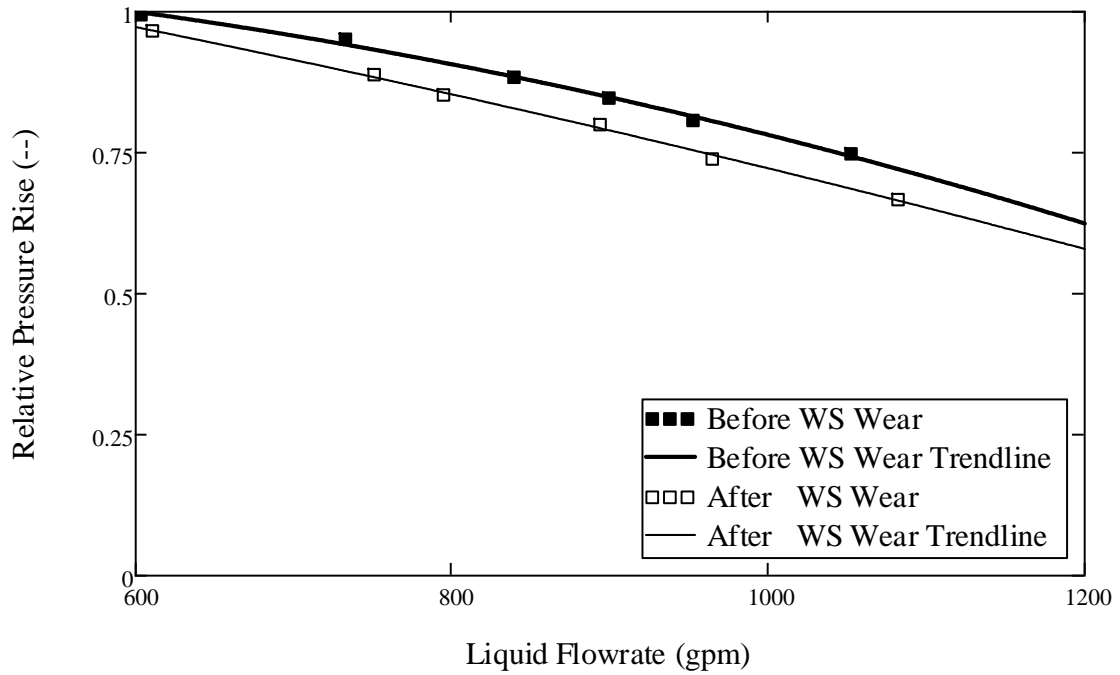(data obtained at 12% GVF)**

Figure 60, Figure 61, and Figure 62 show WAS G400 pressure rise curves before

and after testing for the first, second, and third stage, respectively. Table 12 summarizes

the figures. The first stage showed the most severe pressure degradation. The third

stage showed the least severe pressure degradation. The second stage showed a pressure

degradation in between that shown for the first and third stage. This data confirms what

was found by analyzing the test condition pressure rise data presented in the Test

Condition Per Stage Pressure Rise subsection. The data also confirms that impeller flow

path wear increases with increasing GVF.

Table 12. WAS test average pressure degradation per stage after wear
(data obtained at 12% GVF)

Stage	Average Wear GVF (% w.r.t. stage inlet)	Pressure Degradation (%)
First	20	47.6
Second	17	24.5
Third	10	2.6
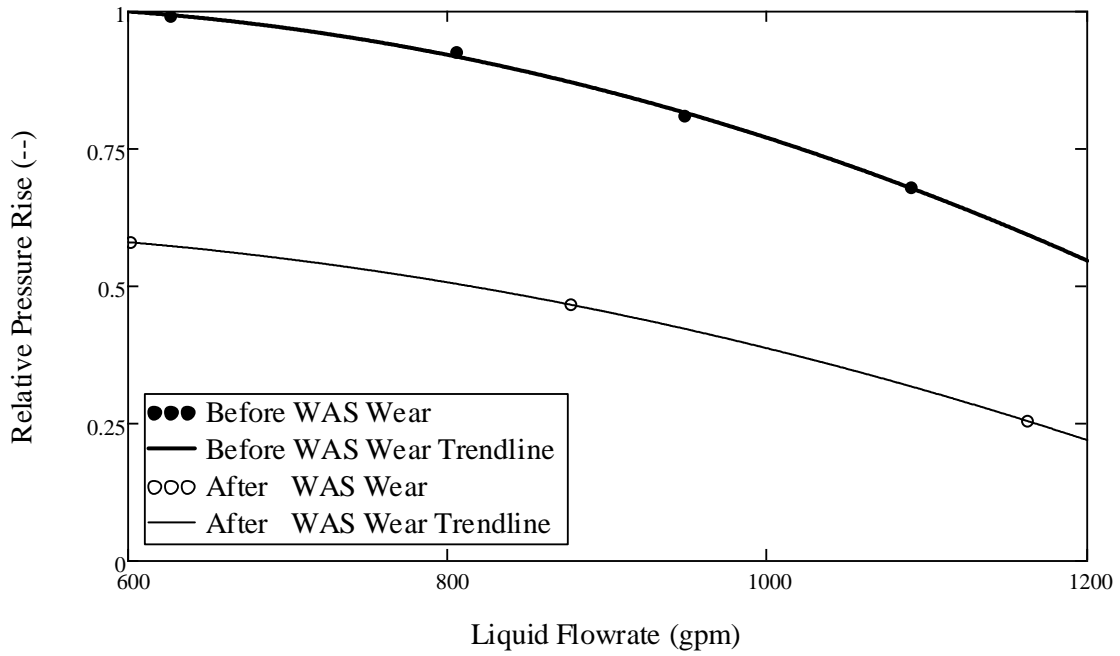
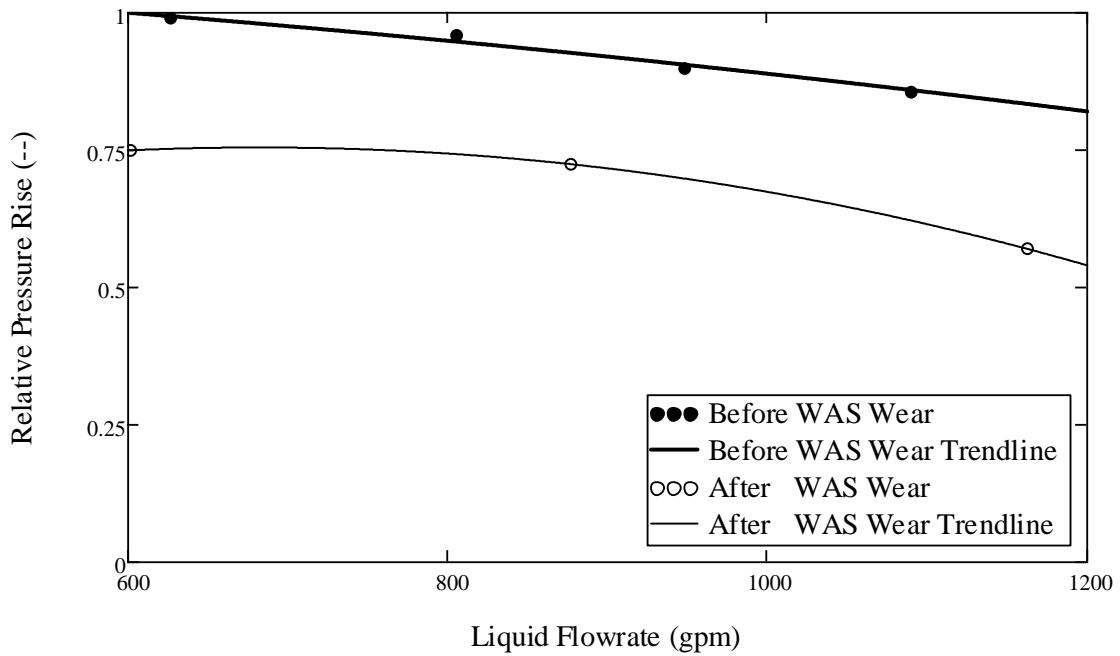**Figure 60. First stage pressure degradation after Water-Air-Sand, WAS, wear (data obtained at 12% GVF)**
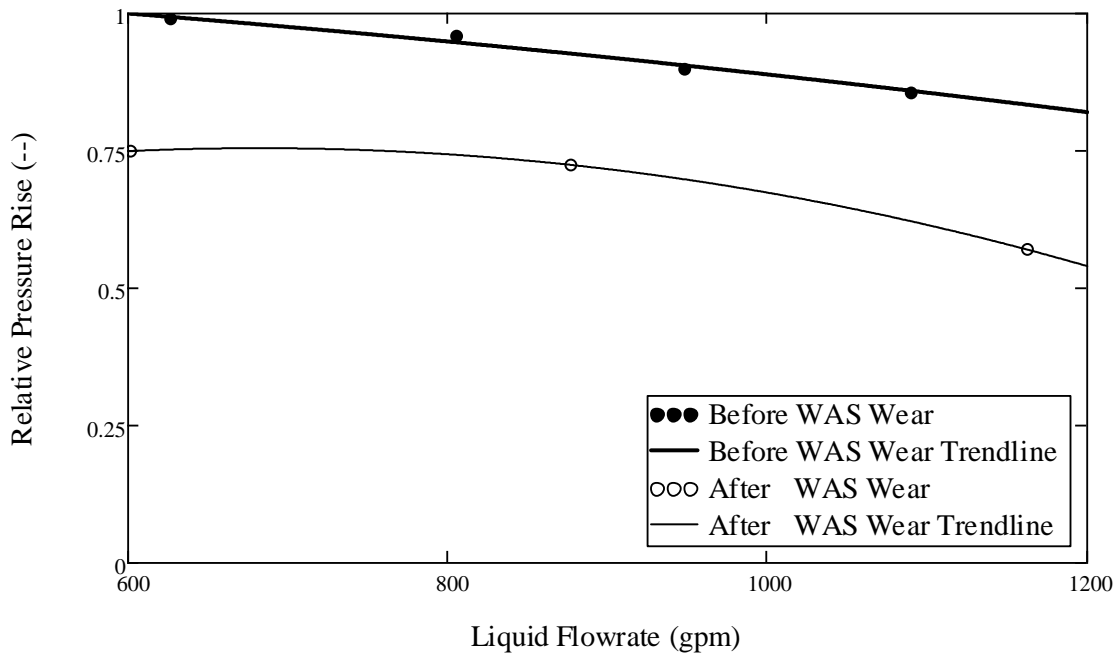
Figure 61. Second stage pressure degradation after Water-Air-Sand, WAS, wear (data obtained at 12% GVF)
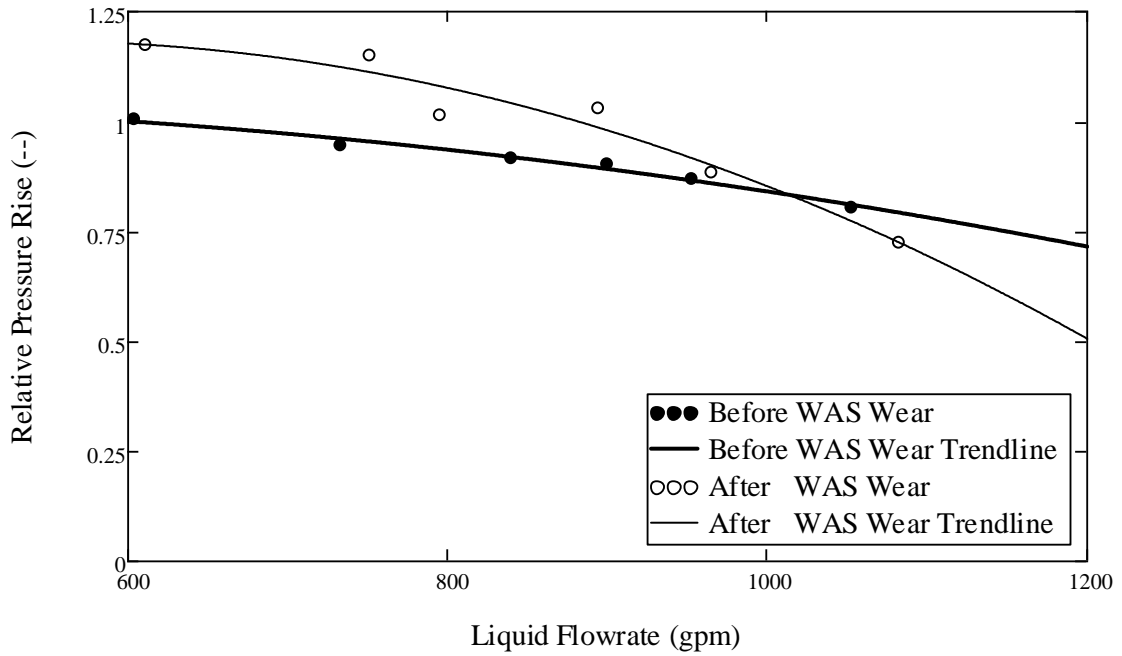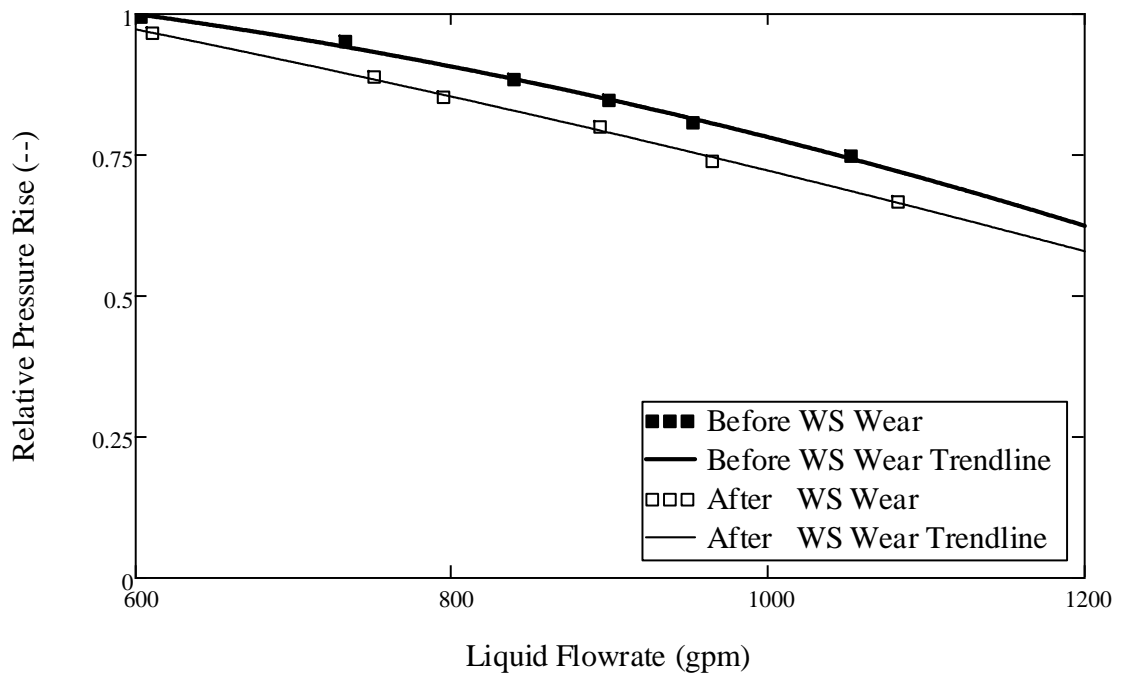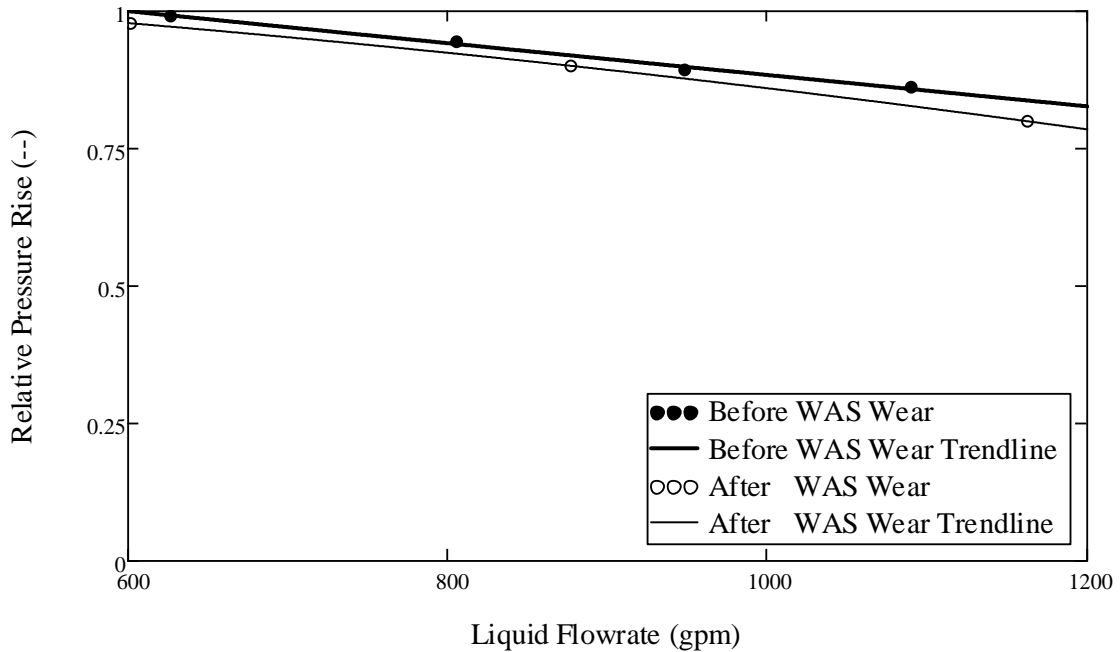
Figure 62. Third stage pressure degradation after Water-Air-Sand, WAS, wear (data obtained at 12% GVF)

Dimensional Measurement Results

This section presents measurement results. The subsections are as follow:

- Second Stage
- Per Stage

Second Stage

Figure 63 and Figure 64 show the metal loss experienced by the impeller and

diffuser for the WS and WAS wear tests. Table 13 summarizes the results. The

measurements confirm that the WAS tested impeller wore more than the WS tested

impeller. The measurements also confirm that the WS tested diffuser wore more than

69

the WAS tested diffuser. Figure 65 through Figure 67 show the front ring seal, back ring seal and radial bearing radial clearance growth for the WS and WAS wear tests. For the WS test, the front and back ring seal clearances grew to a similar gap size. For the WAS test, the front ring seal clearance grew to a larger gap size than the back ring seal clearance. The difference in front versus back ring seal wear is likely caused by impeller imbalance during the WAS testing. The imbalance could have been caused by nonuniform wear and nonuniform flow within the WAS tested impeller. Unbalanced forces would likely be present near the split blade outer members causing the point of unbalanced force application to be nearer the back ring seal than the front ring seal. Due to a lever-like effect, the front ring seal would be pushed farther than the back ring seal because it would be located farther from a virtual fulcrum than the back ring seal. Table 14 summarizes the results presented in the figures. The WAS tested radial bearing experienced more wear than the WS tested bearing. The difference in radial bearing wear was also likely due to the increased impeller imbalance associated with the WAS tested impeller.

Table 13. Second stage impeller and diffuser metal loss after 66 hours of wear

Wear Type	Metal Loss (lb$_f$)					
	Impeller			Diffuser		
Water-Sand, WS	0.83	±	0.01	3.92	±	0.16
Water-Air-Sand, WAS	0.93	±	0.03	2.65	±	0.16
Increase from WS to WAS (%)	11	±	3	-32	±	6

Table 14. Second stage ring seal and radial bearing clearance growth after 66 hours of wear

Wear Type	Radial Clearance Growth (mils)								
	Front Ring Seal			Back Ring Seal			Radial Bearing		
Water-Sand, WS	15.68	±	0.76	18.47	±	0.76	8.01	±	1.41
Water-Air-Sand, WAS	17.89	±	0.76	14.00	±	0.76	13.16	±	1.17
Increase from WS to WAS (%)	14	±	7	-24	±	6	64	±	26
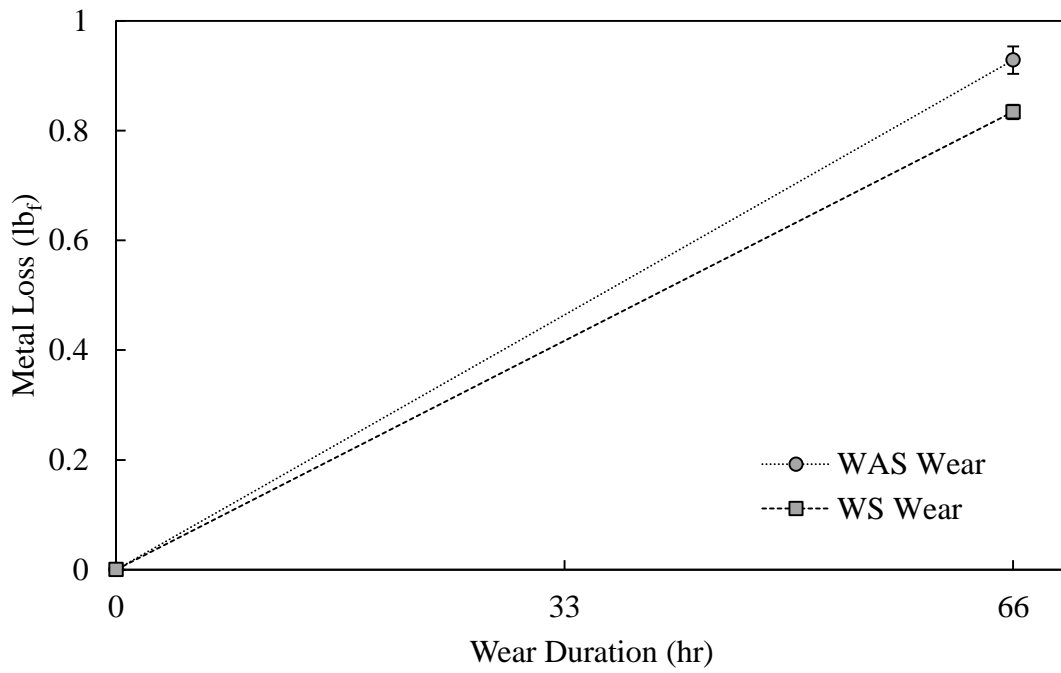
Figure 63. Second stage impeller metal loss
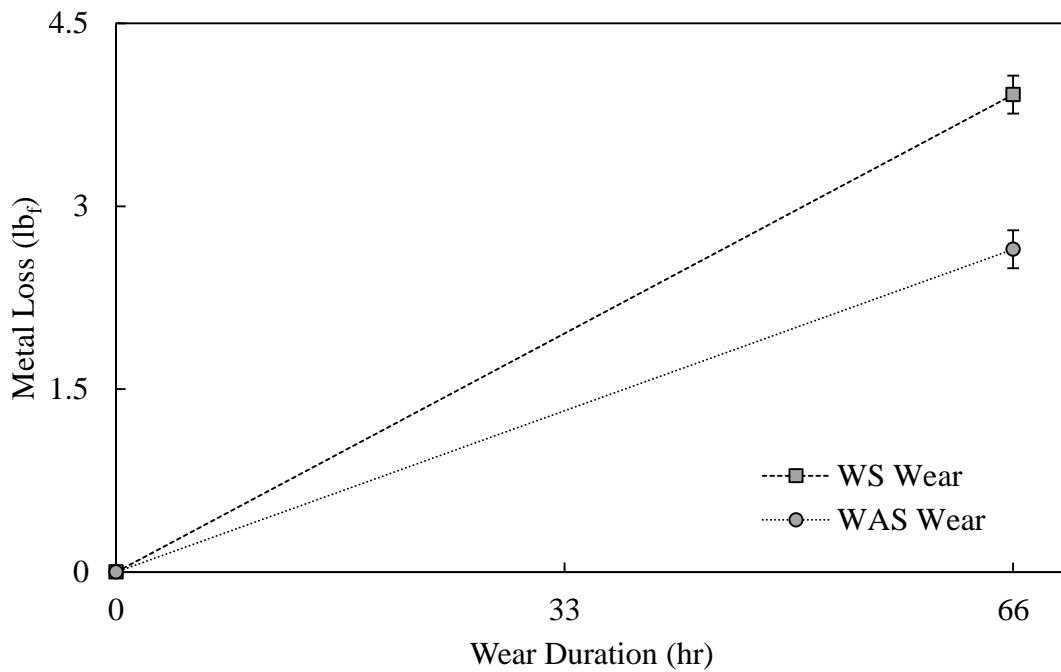
Figure 64. Second stage diffuser metal loss
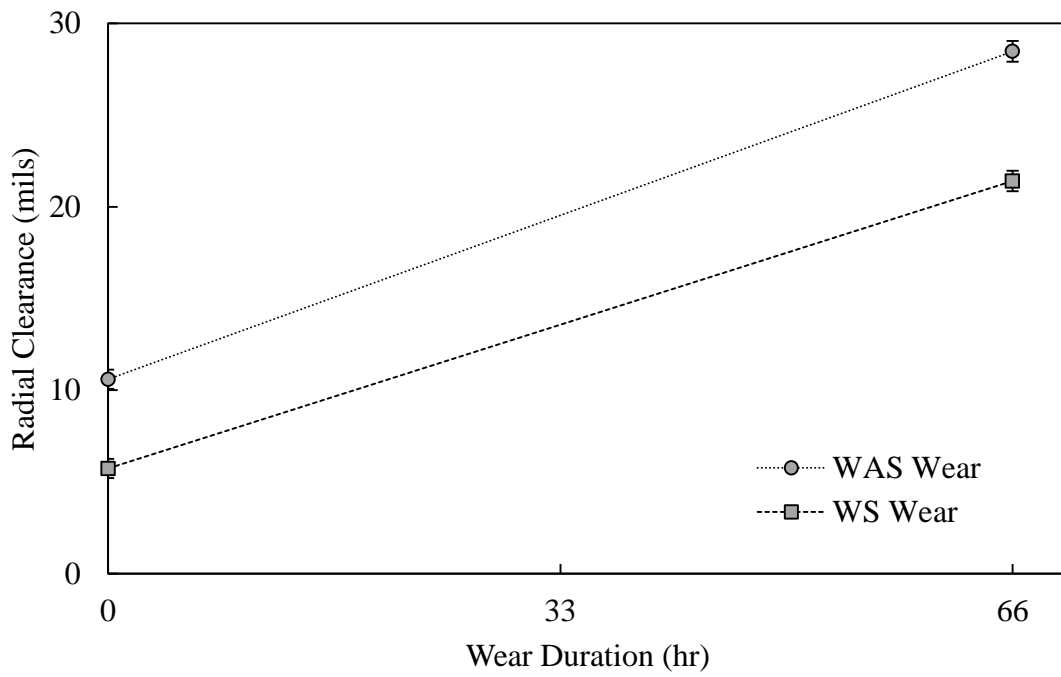
Figure 65. Second stage front ring seal clearance growth
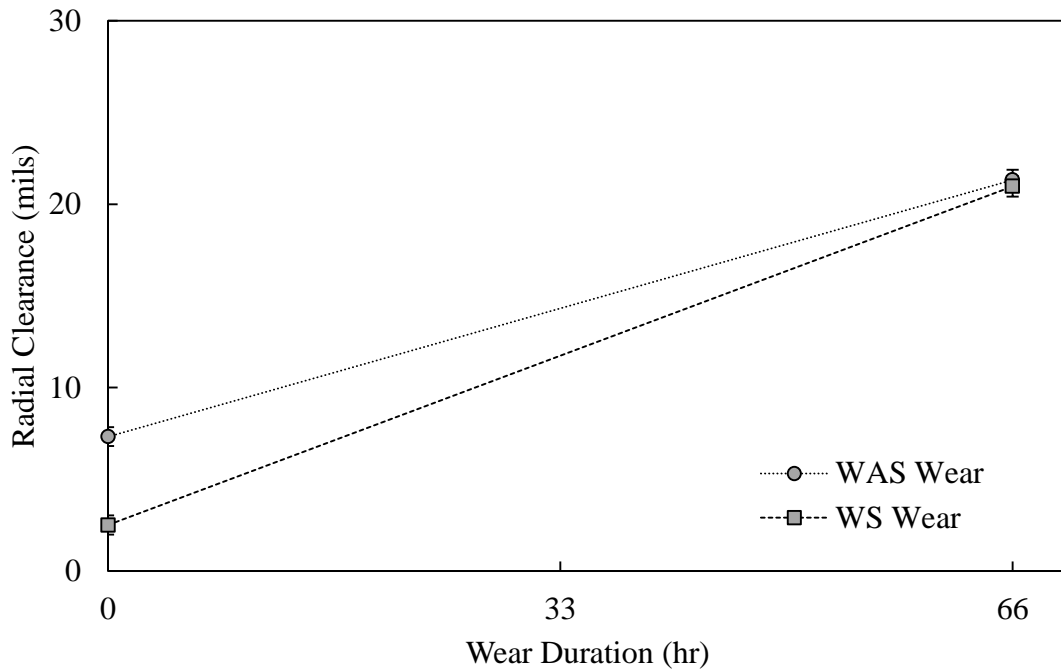
Figure 66. Second stage back ring seal clearance growth
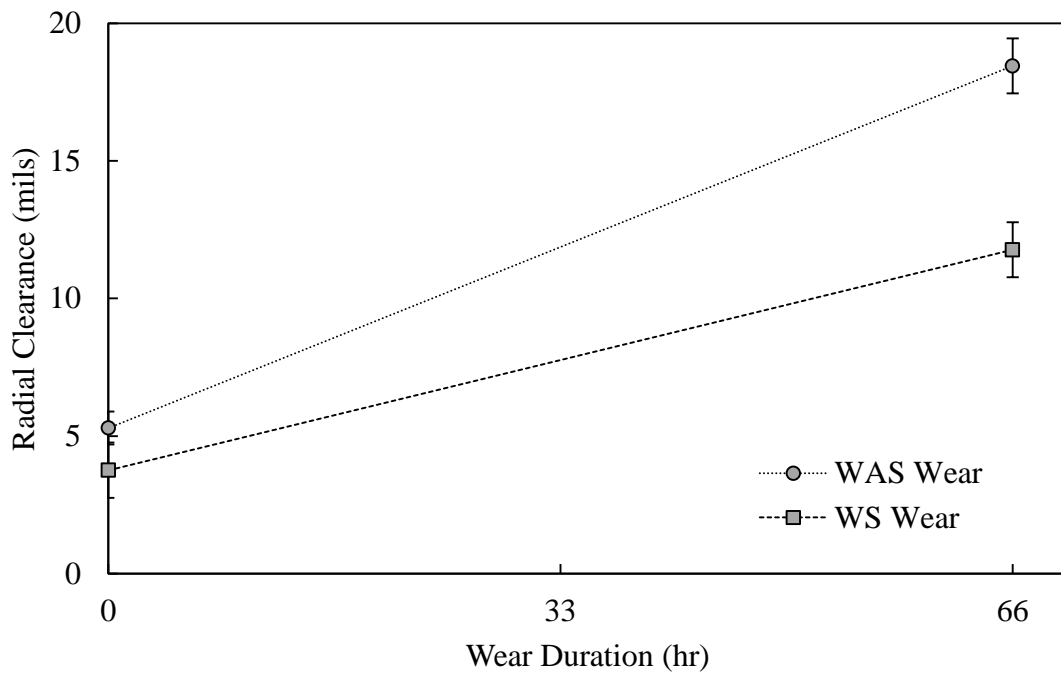
Figure 67. Second stage radial bearing clearance growth

Per Stage

Figure 68 shows the WS and WAS test diffuser metal loss per stage. The data confirms the visual results. Because the diffusers experience various forms of wear, e.g. diffuser flow path wear and internal leakage wear, the data had to be corrected to allow for valid comparison. The impeller metal loss per stage data could not be reasonably corrected to allow for valid comparison because the impellers experienced multiple forms of wear that were highly irregular. Three-dimensional scanning would greatly improve future efforts to quantify pump wear.
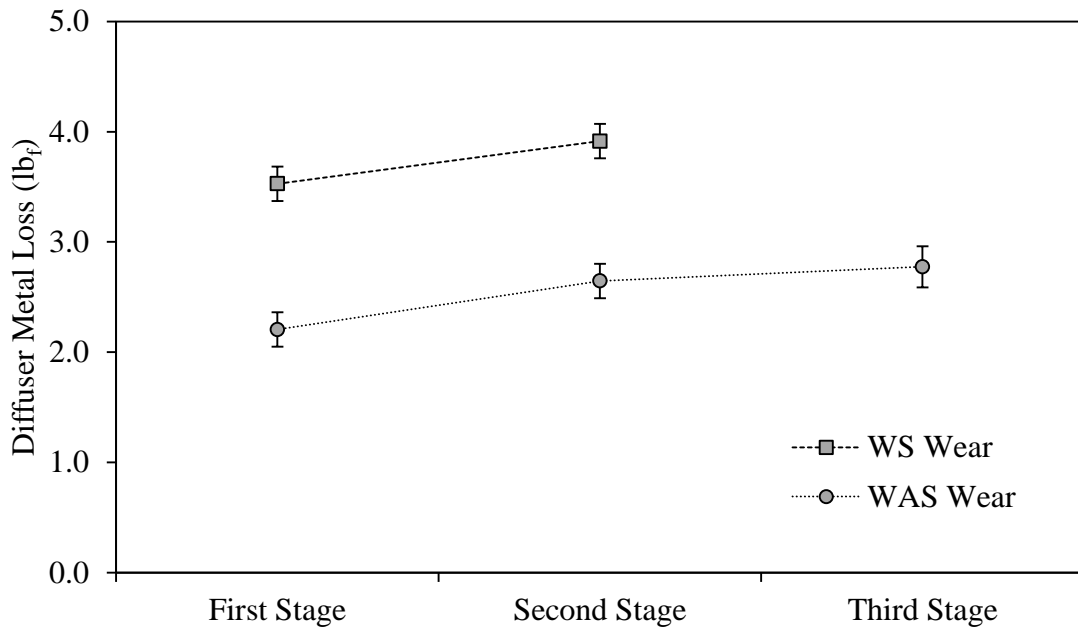
Figure 68. Diffuser metal loss

5. CONCLUSIONS

The following conclusions for Liquid-Gas-Particulate (LGP) and Liquid-Particulate (LP) wear were derived from WS and WAS wear tests. It is believed that WS and WAS wear tests will show the same trends as most LP and LGP wear tests; however, different fluid viscosities could cause wear rates to vary dramatically. The study found that some aspects of LGP pump wear are markedly different than LP pump wear while other aspects are similar. The conclusions of the study are detailed below:

- The pressure side and leading edges of impeller blades and diffuser vanes experience more nonuniform wear for LGP wear than for LP wear. This is caused by nonuniform flow resulting from recirculation zones, predominantly liquid regions, and predominantly gas regions. The recirculation zones could possibly be minimized by a better pump design; however, poor understanding of liquid-gas flows makes this possibility unlikely in the near future.

- Impeller outer member split blade leading and trailing edges as well as impeller hub sidewalls experience more wear during LGP wear than during LP wear. This occurs because predominantly gas regions form at these areas, for LGP flows, and reduce the local fluid viscosity. The reduced viscosity promotes particle escapement and ultimately particle impingement on the impeller surfaces.

- Diffuser inlet sidewall wear is similar for LGP wear and LP wear. This occurs because a predominantly liquid region forms along the sidewall, for LGP flows, and produces a local fluid viscosity similar to the LP flow. The similar fluid

76

viscosities near the sidewall allow particles to escape the LGP and LP flows in a similar fashion.

- Solid particles migrate radially outward in a pumps rotating flow and cause the local particulate concentration along the pump's outer sidewalls to increase through the pump. This causes the wear along the outer sidewalls, particularly near diffuser vane leading edges, to increase through the pump.

- Internal leakage wear is similar for LGP wear and LP wear.

- The pressure degradation for a multiphase stage can be caused by the wear of the stage in question and the wear of previous stages which reduce the inlet pressure and increase the inlet GVF for the stage in question. If the pressure degradation for a multiphase stage is severe, the degradation is likely caused by the wear of the stage in question.

- The way pump performance characteristics change throughout a pump's wear lifecycle were discovered. The power requirement increases and the pressure rise decreases as ring seal surfaces wear; however, the power requirement and the pressure rise decrease as impeller blades wear through their thicknesses. Efficiency is primarily a function of ring seal surface wear. The power requirement decrease due to through thickness impeller blade wear dominates the power requirement rise due to ring seal surface wear. A pump will likely wear its ring seals before it will wear through the thickness of its impeller blades. During a pumps wear lifecycle, a pump will initially start requiring slightly more power; later on, the pump will start requiring significantly less power. A pump

will also steadily decrease in efficiency in proportion to its ring seal clearance. Furthermore, a pump will initially start to slightly decrease its pressure rise; later on, a pump will start to significantly decrease its pressure rise.

- Pump wear lifecycles progresses faster for LGP wear than LP wear.

- Ring seal and radial bearings experience more wear during LGP wear than during LP wear. This is caused by impeller imbalance resulting from nonuniform wear and nonuniform flow within the LGP impellers.

- If ESP wear rates are desired to be estimated, a fluid significantly more viscous than water should be used because crude oil is often significantly more viscous than water.

- Three-dimensional scanning would greatly improve future efforts to quantify pump wear. This is the case because turbine pump geometry is very complex and difficult to measure with traditional tools, wear patterns tend to be highly irregular, and pump components often perform multiple functions and exhibit multiple forms of wear (e.g. the impeller imparts energy to the fluid and seals internal leakage, these functions cause the impeller to experience flow path wear and internal leakage wear).

REFERENCES

[1] C. Dunham, "27th ESP Workshop: Summary of Presentations," Oilfield Automation Consulting, 1 May 2013. [Online]. Available: http://www.spegcs.org/media/files/files/cebfcc3a/2013-ESP-Workshop-Summary-of-Presentations.pdf. [Accessed 26 May 2014].

[2] G. Takacs, Electrical Submersible Pump Manual: Design, Operations, and Maintenance, Burlington, MA: Gulf Professional Publishing, 2009, pp. 1-5, 128-129, 155-164.

[3] Europump and Hydraulic Institute, Pump Life Cycle Costs, Parsippany, NJ: Hydraulic Institute, 2001.

[4] S. Noonan, "Electric Submersible Pump (ESP) Reliability," in *Society of Petroleum Engineers Webinar*, Houston, TX, 2013.

[5] V. Chernikov, "Evaluating ESP Reliability to Increase Non-Failure Operations," Oil & Gas Eurasia, 29 March 2013. [Online]. Available: http://www.oilandgaseurasia.com/en/tech_trend/evaluating-esp-reliability-increase-non-failure-operations. [Accessed 5 May 2014].

[6] M. S. Raymond and W. L. Leffler, Oil and Gas Production: in Nontechnical Language, Tulsa, OK: Penn Well Corporation, 2006, pp. 172-174.

[7] P. Cooper, "Tutorial on Multiphase Gas-Liquid Pumping," in *International Pump Users Symposium*, Houston, TX, 1996.

[8] American Turbine, "Installation and Operation of American Turbine Pumps," 1 January 1997. [Online]. Available: http://americanturbine.net/manual/installation. [Accessed 1 May 2014].

[9] J. F. Gülich, Centrifugal Pumps, New York, NY: Springer, 2010.

[10] R. Magiera, "Computational Fluid Dynamics for Fans and Plants," Ventilatorenfabrik Oelde GmbH, 1 September 2010. [Online]. Available: http://www.venti-oelde.com/uploads/tx_sbdownloader/stroemungssim-en.pdf. [Accessed 15 May 2014].

[11] O. Petit, M. Page, M. Beaudoin and H. Nilsson, "The ERCOFTAC Centrifugal Pump OpenFOAM Case-Study," in *3rd IAHR International Meeting of the Workgroup on Cavitation and Dynamic Problems in Hydraulic Machinery and Systems*, Brno, Czech Republic, 2009.

[12] W. Marscher, ASM Handbook: Friction, Lubrication, and Wear Technology: Wear of Pumps, vol. 18, Materials Park, OH: ASM International, 1992, pp. 593-601.

[13] I. J. Karassik, J. P. Medina, P. Cooper and C. C. Heald, Pump Handbook, New York, NY: McGraw Hill, 2008.

[14] Flygt, Slurry Handbook: Guidelines for Slurry Pumping, Trosa, Sweden: Trosa Tryckeri AB, 2002.

[15] G. Stobie, R. Hart, S. Svedeman and K. Zanker, "Erosion in a Venturi Meter with Laminar and Turbulent Flow and Low Reynolds Number Discharge Coefficient Measurements," in *25th International North Sea Flow Measurement Workshop*, Oslo, Norway, 2007.

[16] J. Evans, "A Brief Introduction to Centrifugal Pumps," Pacific Liquid & Air Systems, 1 January 1990. [Online]. Available: http://www.pacificliquid.com/pumpintro.pdf. [Accessed 18 May 2014].

[17] J. Caridad and F. Kenyery, "CFD Analysis of Electric Submersible Pumps (ESP) Handling Two-Phase Mixtures," *Energy Resources Technology,* vol. 126, pp. 99-104, 2004.

[18] B. Murthy, R. Ghadge and J. Joshi, "CFD Simulations of Gas–Liquid–Solid Stirred Reactor: Prediction of Critical Impeller Speed for Solid Suspension," *Chemical Engineering Science,* vol. 62, pp. 7184-7195, 2007.

[19] H. Casillas, Interviewee, *Email Correspondance.* [Interview]. 19 May 2014.

[20] S. Klein, "Engineering Equation Solver," F Chart Software, Madison, WI, 2013.

[21] Enbridge Pipelines Inc., "2013 Crude Characteristics No. 44," Enbridge Energy Partners, L.P., 24 March 2013. [Online]. Available: http://www.enbridge.com/~/media/www/Site%20Documents/Delivering%20Energy/2013%20Crude%20Characteristics.pdf. [Accessed 27 May 2014].

[22] A. L. Kao, "Submersible Pump Impeller Design for Lifting Gaseous Fluid". United States Patent 6,676,366 B2, 13 January 2004.

[23] Schlumberger, "High-Efficiency ESP Pumps," Schlumberger Limited, 1 January 2013. [Online]. Available: http://www.slb.com/services/production/artificial_lift/submersible/esp_components /high_efficiency_pumps.aspx. [Accessed 30 May 2014].

[24] Imajey Consulting Engineers Pvt. Ltd., "Centrifugal Pump," Learn Engineering, 21 February 2013. [Online]. Available: http://www.learnengineering.org/2013/03/centrifugal-pump.html. [Accessed 1 April 2014].

[25] R. E. A. Arndt, S. Paul and C. R. Ellis, "Investigation of the Use of Air Injection to Mitigate Cavitation Erosion," University of Minesota, Minneapolis, MN, 1993.

[26] Centrilift, Catalog Pump Curves, Claremore, OK: Baker Hughes, 2013.

[27] R. Covert, "Properties and Applications of Ni-Resist and Ductile Ni-Resist Alloys," Nickel Institute, Toronto, Canada, 1998.

[28] L. W. Mays, Water Distribution Systems Handbook, New York: McGraw Hill, 2000, p. 5.15.

[29] N. C. Diaz, "Effects of Sand on the Components and Performance of Electric Submersible Pumps," Texas A&M University, College Station, TX, 2012.

[30] PIP, PIC001 Piping and Instrumentation Diagram Documentation Criteria, Austin, TX: Process Industry Practices, 2000.